NASA TECHNICAL MEMORANDUM
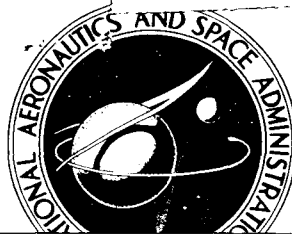
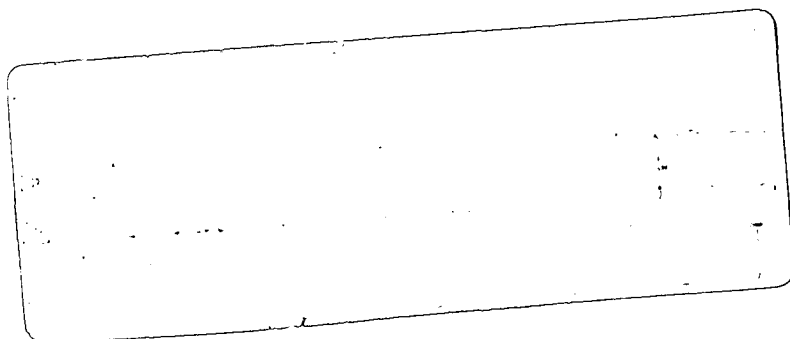# AERODYNAMIC CHARACTERISTICS AT MACH 1.60, 2.00, AND 2.50 OF A CRUCIFORM MISSILE CONFIGURATION WITH IN-LINE TAIL CONTROLS

by William A. Corlett and Dennis E. Fuller

Langley Research Center
Langley Station, Hampton, Va.

NATIONAL AERONAUTICS AND SPACE ADMINISTRATION • WASHINGTON, D. C. • JULY 1965

AERODYNAMIC CHARACTERISTICS AT MACH 1.60, 2.00, AND 2.50

OF A CRUCIFORM MISSILE CONFIGURATION WITH

IN-LINE TAIL CONTROLS

By William A. Corlett and Dennis E. Fuller

Langley Research Center
Langley Station, Hampton, Va.

NATIONAL AERONAUTICS AND SPACE ADMINISTRATION

AERODYNAMIC CHARACTERISTICS AT MACH 1.60, 2.00, AND 2.50

OF A CRUCIFORM MISSILE CONFIGURATION WITH

IN-LINE TAIL CONTROLS[*]

By William A. Corlett and Dennis E. Fuller
Langley Research Center

SUMMARY

An investigation has been conducted at Mach numbers of 1.60, 2.00, and 2.50 to determine the aerodynamic characteristics of a cruciform missile configuration with low-aspect-ratio wings and in-line tail controls close-coupled with the wings. Hinge-moment characteristics were also obtained for various control deflections.

The results indicate that the model was longitudinally and directionally stable about the selected center-of-gravity location at all test Mach numbers, although there was a significant reduction in stability levels with increase in Mach number. The vertical tail surfaces produced effective yaw and roll control at all test Mach numbers and angles of attack, although some nonlinear characteristics occurred at high angles of attack because of differences in effectiveness of the top and bottom tail surfaces.

INTRODUCTION

One of the primary aerodynamic requirements of an air-to-surface missile is that it possess an adequate stability level over its operational range with regard to angles of attack and sideslip as well as Mach numbers. From the control consideration, it is also desirable that the missile be able to operate at a small stability margin with no inherent control reversal introduced by aerodynamic nonlinearities. Numerous missile configurations with various control devices have been investigated by the National Aeronautics and Space Administration and the experimental results for some of these configurations are presented in references 1 to 11.

As a continuation of the study of various missile concepts, the present investigation is concerned with the determination of the aerodynamic characteristics of a missile with cruciform, low-aspect-ratio wings and in-line tail surfaces close-coupled with the wings.

The model with various control deflections has been investigated in the Langley Unitary Plan wind tunnel, and the results obtained at Mach numbers of 1.60, 2.00, and 2.50 are presented herein. Measurements of tail-surface hinge moments are also included. The tests were made at a constant Reynolds number per foot of 2.0×10^6, at angles of attack from about $-4°$ to $22°$, and at angles of sideslip from about $-5°$ to $9°$.

SYMBOLS

The aerodynamic-coefficient data are referred to the body-axis system. The moment reference was located at a station 44.8 percent of the body length from the nose.

A   reference area, 0.07792 sq ft

C_A axial-force coefficient, $\dfrac{\text{Axial force}}{qA}$

C_h hinge-moment coefficient, $\dfrac{\text{Hinge moment}}{qAd}$

$C_{h,1}$ hinge-moment coefficient of right horizontal tail

$C_{h,2}$ hinge-moment coefficient of bottom vertical tail

$C_{h,3}$ hinge-moment coefficient of left horizontal tail

$C_{h,4}$ hinge-moment coefficient of top vertical tail

C_l rolling-moment coefficient, $\dfrac{\text{Rolling moment}}{qAd}$

C_{l_β} effective dihedral parameter, $\dfrac{\partial C_l}{\partial \beta}$, per degree

C_m pitching-moment coefficient, $\dfrac{\text{Pitching moment}}{qAd}$

C_{m_α} longitudinal stability parameter, $\dfrac{\partial C_m}{\partial \alpha}$ near $\alpha = 0°$, per degree

C_N normal-force coefficient, $\dfrac{\text{Normal force}}{qA}$

C_n yawing-moment coefficient, $\dfrac{\text{Yawing moment}}{qAd}$

C_Y side-force coefficient, $\dfrac{\text{Side force}}{qA}$

d   reference body diameter, 3.780 in.

M   free-stream Mach number

q   free-stream dynamic pressure

α angle of attack, deg

β angle of sideslip, deg

δ_1 control deflection of right horizontal tail (viewed from downstream), negative leading edge down, deg

δ_2 control deflection of bottom vertical tail, negative leading edge to left (viewed from downstream), deg

δ_3 control deflection of left horizontal tail (viewed from downstream), negative leading edge down, deg

δ_4 control deflection of top vertical tail, negative leading edge to left (viewed from downstream), deg

<div align="center">MODEL</div>

Dimensional details of the model are shown in figure 1, and the model mounted in the test section is shown in figure 2.

The body, which was composed of a von Kármán forebody, a cylindrical mid-section, and a boattailed afterbody, had a fineness ratio of 9.57. The cruci-form trapezoidal wings had rounded leading edges, beveled trailing edges, and a maximum thickness-chord ratio of 0.04. A strake extended from each wing leading edge to a station on the forebody corresponding to 19.9 percent of the body length. Each wing panel, excluding the strake, had an exposed area of 26.66 sq in. The wings were located so that the center of area was at a point corresponding to 62.9 percent of the body length.

The cruciform tail surfaces, which were in-line and close-coupled with the wings, are identified as 1, 2, 3, and 4. The numbering begins with the hori-zontal surface on the right (viewed from downstream) and goes clockwise. Thus, the bottom and top vertical tail surfaces will be identified with the numbers 2 and 4, respectively, and the right and left horizontal tail surfaces will be identified with the numbers 1 and 3, respectively. The horizontal tails had a maximum thickness-chord ratio of 0.10 and the vertical tails had a maximum thickness-chord ratio of 0.05. Pitch control was provided by movement of the two horizontal tail surfaces, and lateral and directional control was provided by movement of the two vertical tail surfaces. The exposed area of each tail

surface was 8.35 sq in. The center of area of the all-movable tails was located at a point corresponding to 88.9 percent of the body length. Each tail was provided with a strain-gage balance to measure hinge moments about a hinge line located 11.72 percent root chord forward of the center of area.

The model was also provided with two simulated support brackets located so as to allow the missile to be carried, prior to launch, in a 45° rolled position. (See fig. 1.)

TESTS, CORRECTIONS, AND ACCURACY

The tests were conducted in the low Mach number test section of the Langley Unitary Plan wind tunnel, which is a continuous-flow, variable-pressure facility. The test section is about 4 by 4 feet in cross section and about 7 feet in length. The nozzle leading to the test section is of the asymmetric sliding-block type which permits continuous variation in Mach number from 1.47 to 2.86. The model was mounted in the tunnel on a remote-controlled sting, and forces and moments were measured by means of a six-component, electrical strain-gage balance mounted internally.

For all tests, the Reynolds number per foot was 2.0×10^6. The dewpoint, measured at stagnation pressure, was maintained below -30° F to prevent condensation effects. The stagnation temperature was 150° F whereas the stagnation pressure varied as follows for the three test Mach numbers:

Mach number	Stagnation pressure, psia
1.60	7.92
2.00	9.20
2.50	11.73

Tests were made through an angle-of-attack range from approximately -4° to 22° and through an angle-of-sideslip range from approximately -5° to 9° at angles of attack of about 0°, 11°, and 22°. The angles of attack and sideslip have been corrected for tunnel airflow misalinement and for deflection of the balance and sting due to aerodynamic loads. The balance-chamber pressure was measured by means of a single static-pressure orifice located in the vicinity of the balance and the results have been adjusted to correspond to free-stream static pressure acting over the model base.

In order to assure boundary-layer transition to turbulent conditions, 1/16-inch-wide strips of No. 60 carborundum grit were placed streamwise 1/2 inch aft of the nose and 1/2 inch aft of the leading edges of the wings and tails.

Based on balance calibration and data repeatability, the data presented herein are estimated to be accurate within the following limits:

$$C_A \ . \ \pm 0.015$$
$$C_N \ . \ \pm 0.09$$
$$C_m \ . \ \pm 0.03$$
$$C_n \ . \ \pm 0.03$$
$$C_l \ . \ \pm 0.02$$
$$C_Y \ . \ \pm 0.04$$
$$C_h \ . \ \pm 0.001$$
$$M \ . \ \pm 0.015$$
$$\alpha, \ deg \ . \ \pm 0.1$$
$$\beta, \ deg \ . \ \pm 0.1$$

DISCUSSION OF RESULTS

Longitudinal Aerodynamic Characteristics

The longitudinal aerodynamic characteristics of the model with various pitch-control deflections and with the horizontal tails removed are presented in figure 3. The results indicate that the model is stable about the selected center-of-gravity location and has positive pitch-control effectiveness at all test angles of attack for each Mach number in the investigation. Pitch-control effectiveness appears to be linear with tail-deflection angle near $0°$ angle of attack for each test Mach number. However, at Mach numbers 2.00 and 2.50, a noticeable decrease in tail effectiveness occurs with increase in angle of attack. There is a decrease in the value of C_{m_α} of about 0.13, and a reduction in pitch-control effectiveness of about 40 percent between Mach numbers of 1.60 and 2.50.

Lateral Aerodynamic Characteristics

The effect of vertical-control-surface deflections on the aerodynamic characteristics in sideslip of the model with pitch-control settings of $0°$ and $-20°$ is presented in figures 4 and 5, respectively. A comparison of the data in figures 4 and 5 indicates that with the exception of variations in rolling moment at the higher Mach numbers there are only slight effects on the sideslip characteristics as a result of deflecting the pitch-control surfaces to $-20°$.

With all control surfaces set at $0°$ (fig. 4), the model is directionally stable at each test Mach number, although there is a decrease in directional stability with increase in Mach number from 1.60 to 2.50. Values of C_{l_β} show no appreciable effect of Mach number at an angle of attack of $0°$ but do indicate a large effect of angle of attack wherein, with increasing angle of attack, values of C_{l_β} initially become more negative and then reverse to positive. (See figs. 4(c), 4(d), and 4(e), for example.) There are no significant effects of sideslip angle on roll- and yaw-control effectiveness at any of the test Mach numbers or angles of attack.

Some effects of angle of attack on the configuration with various control settings are more clearly shown in figures 6 and 7 where the data for $\beta = 0^\circ$ for the lateral coefficients are plotted as a function of angle of attack for each Mach number. For $\delta_1 = \delta_3 = 0^\circ$ or -20° an angle of sideslip of 0° (figs. 6 and 7), the vertical control surfaces deflected symmetrically $\left(\delta_2 = -10^\circ, \; \delta_4 = -10^\circ\right)$ produce effective C_n at all test Mach numbers although there is a decrease in effectiveness of about 50 percent at $\alpha = 0^\circ$ between $M = 1.60$ and $M = 2.50$. This yawing-moment effectiveness is produced with only small effects on rolling moment except at high angles of attack for $M = 2.00$ and $M = 2.50$ where a positive increment in roll occurs. There is also little change in yaw effectiveness for the symmetrical deflection of δ_2 and δ_4 with increase in angle of attack (figs. 6 and 7).

The yawing moment obtained with a -20° deflection of the top vertical tail only $\left(\delta_4\right)$ is approximately the same at $\alpha = 0^\circ$ as that obtained with a -10° deflection of the top and bottom tails together $\left(\delta_2 \text{ and } \delta_4\right)$. With increasing angle of attack, however, the effectiveness of the top tail decreases rapidly at the higher Mach numbers as a result of the adverse effects of the wing-body wake, and the yawing moment produced by deflection of the top tail alone becomes considerably less than that produced by combined deflection of the top and bottom tails. (See figs. 6 and 7.)

Differential vertical-control-surface deflections lead to positive roll-control effectiveness $\left(-C_{l_\beta}\right)$ at all test Mach numbers and angles of attack. At each Mach number and particularly at high angles of attack, differential settings of $+10^\circ$ and -10° on the vertical surfaces provide greater rolling-moment values than do settings of 0° and -20°, partly because of the decrease in effectiveness of the top vertical surface and partly because of an increase in effectiveness of the bottom vertical surface. As would be expected at $\alpha = 0^\circ$, differential deflections of 0° and -20° result in a positive increment in yawing moment whereas the equal but opposite deflections of 10° result in essentially no yawing moment. (See figs. 6 and 7.) With increasing angle of attack at $M = 2.00$ and $M = 2.50$, however, the 0° and -20° deflections provide a less positive increment in C_n and the $+10^\circ$ and -10° deflections begin to provide an increasingly negative C_n for $\delta_1 = \delta_3 = 0^\circ$ (fig. 6) as a result of the difference in effectiveness between the top and bottom tails. However, for $\delta_1 = \delta_3 = -20^\circ$ (fig. 7), the $+10^\circ$ and -10° deflections begin to provide an increasingly positive C_n with increasing angle of attack for $M = 2.00$ and $M = 2.50$.

Hinge-Moment Characteristics

Hinge-moment coefficients for the control surfaces at various deflection angles are presented in figures 8 and 9. The results, in general, indicate negative variations of C_h with increasing angle of attack and with positive control deflection and a decrease in C_h with increasing Mach number.

CONCLUSIONS

An investigation was conducted at Mach numbers of 1.60, 2.00, and 2.50 to determine the aerodynamic characteristics of a cruciform missile configuration with low-aspect-ratio wings and close-coupled in-line tail controls at various defl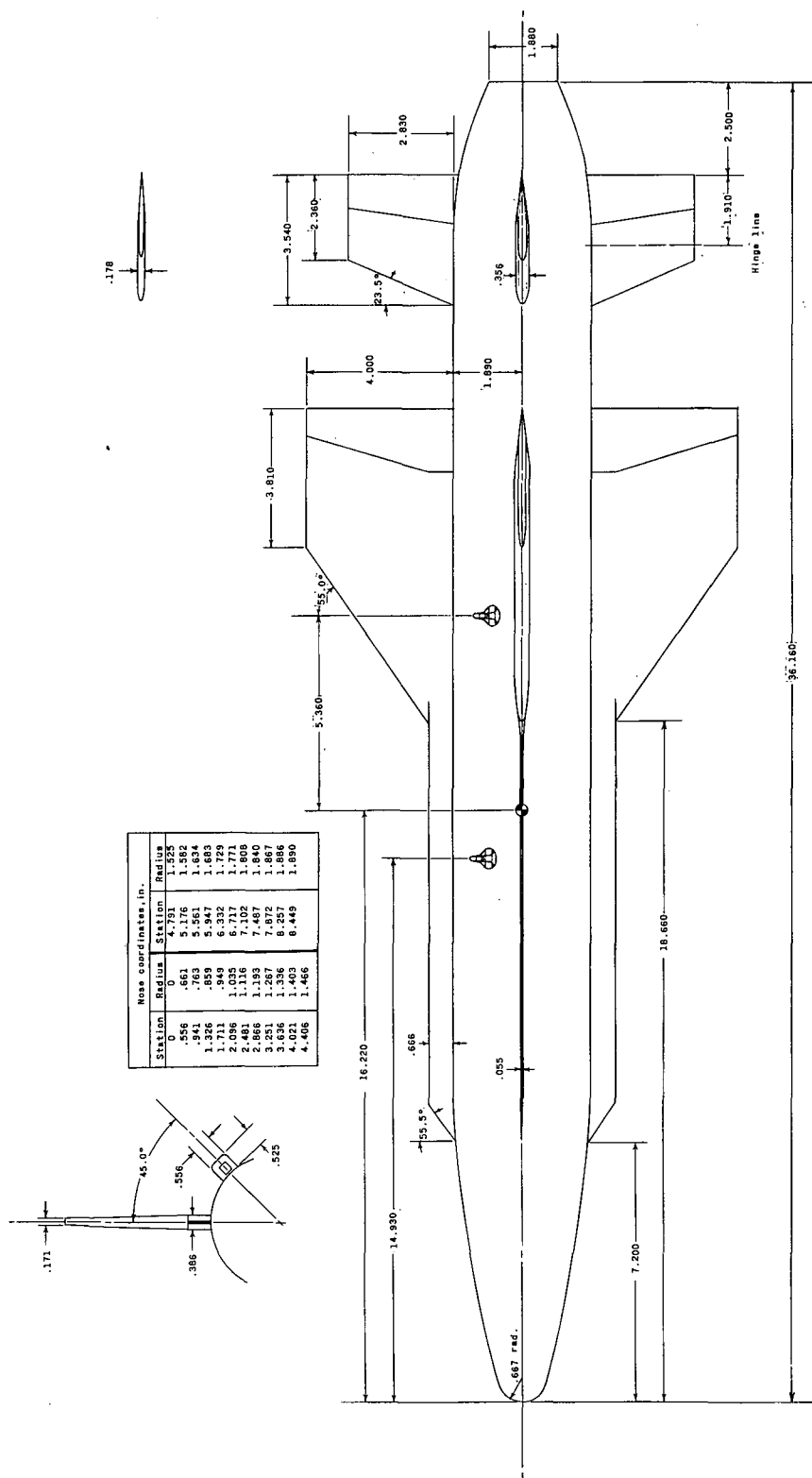ection angles. Hinge-moment characteristics were also obtained for various control deflections. Results of the investigation lead to the following conclusions:

1. The model was longitudinally and directionally stable about the selected center-of-gravity location at all test Mach numbers, although there was a significant reduction in stability with increase in Mach number.

2. The vertical tail surfaces produced effective yaw and roll control at all test Mach numbers and angles of attack although some nonlinear characteristics occurred at high angles of attack because of differences in effectiveness of the top and bottom tail surfaces.

3. Deflection of the pitch-control surfaces generally led to only small effects on the roll- and yaw-control characteristics of the model.

Langley Research Center,
    National Aeronautics and Space Administration,
        Langley Station, Hampton, Va., April 23, 1965.

REFERENCES

1. Stone, David G.: Maneuver Performance of Interceptor Missiles. NACA RM L58E02, 1958.

2. Robinson, Ross B.: Aerodynamic Characteristics of Missile Configurations With Wings of Low Aspect Ratio for Various Combinations of Forebodies, Afterbodies, and Nose Shapes for Combined Angles of Attack and Sideslip at a Mach Number of 2.01. NACA RM L57D19, 1957.

3. Robinson, Ross B.: Wind-Tunnel Investigation at a Mach Number of 2.01 of the Aerodynamic Characteristics in Combined Angles of Attack and Sideslip of Several Hypersonic Missile Configurations With Various Canard Controls. NACA RM L58A21, 1958.

4. Turner, Kenneth L.; and Appich, W. H., Jr.: Investigation of the Static Stability Characteristics of Five Hypersonic Missile Configurations at Mach Numbers From 2.29 to 4.65. NACA RM L58D04, 1958.

5. Spearman, M. Leroy; and Robinson, Ross B.: Longitudinal Stability and Control Characteristics at Mach Numbers of 2.01, 4.65, and 6.8 of Two Hypersonic Missile Configurations, One Having Low-Aspect-Ratio Cruciform Wings With Trailing-Edge Flaps and One Having a Flared Afterbody and All-Movable Controls. NASA TM X-46, 1959.

6. Robinson, Ross B.; and Bernot, Peter T.: Aerodynamic Characteristics at a Mach Number of 6.8 of Two Hypersonic Missile Configurations, One With Low-Aspect-Ratio Cruciform Fins and Trailing-Edge Flaps and One With a Flared Afterbody and All-Movable Controls. NACA RM L58D24, 1958.

7. Church, James D.; and Kirkland, Ida M.: Static Aerodynamic Characteristics of Several Hypersonic Missile-and-Control Configurations at a Mach Number of 4.65. NASA TM X-187, 1960.

8. Robinson Ross B.; and Spearman, M. Leroy: Aerodynamic Characteristics for Combined Angles of Attack and Sideslip of a Low-Aspect-Ratio Cruciform-Wing Missile Configuration Employing Various Canard and Trailing-Edge Flap Controls at a Mach Number of 2.01. NASA MEMO 10-2-58L, 1958.

9. Robinson, Ross B.; and Foster, Gerald V.: Static Longitudinal Stability and Control Characteristics at a Mach Number of 2.01 of a Hypersonic Missile Configuration Having All-Movable Wing and Tail Surfaces. NASA TM X-516, 1961.

10. Ulmann, Edward F.; and Ridyard, Herbert W.: Flow-Field Effects on Static Stability and Control at High Supersonic Mach Numbers. NACA RM L55L19a, 1956.

11. Fuller, Dennis E.; and Corlett, William A.: Supersonic Aerodynamic Characteristics of a Cruciform Missile Configuration With Low-Aspect-Ratio Wings and In-Line Tail Controls. NASA TM X-1025, 1964.

Nose coordinates, in.

Station	Radius	Station	Radius
0	0	4.791	1.525
.556	.661	5.176	1.582
.941	.763	5.561	1.634
1.326	.859	5.947	1.683
1.711	.949	6.332	1.729
2.096	1.035	6.717	1.771
2.481	1.116	7.102	1.808
2.866	1.193	7.487	1.840
3.251	1.267	7.872	1.867
3.636	1.336	8.257	1.886
4.021	1.403	8.449	1.890
4.406	1.466		

Figure I. - Model details. (All dimensions are in inches.)
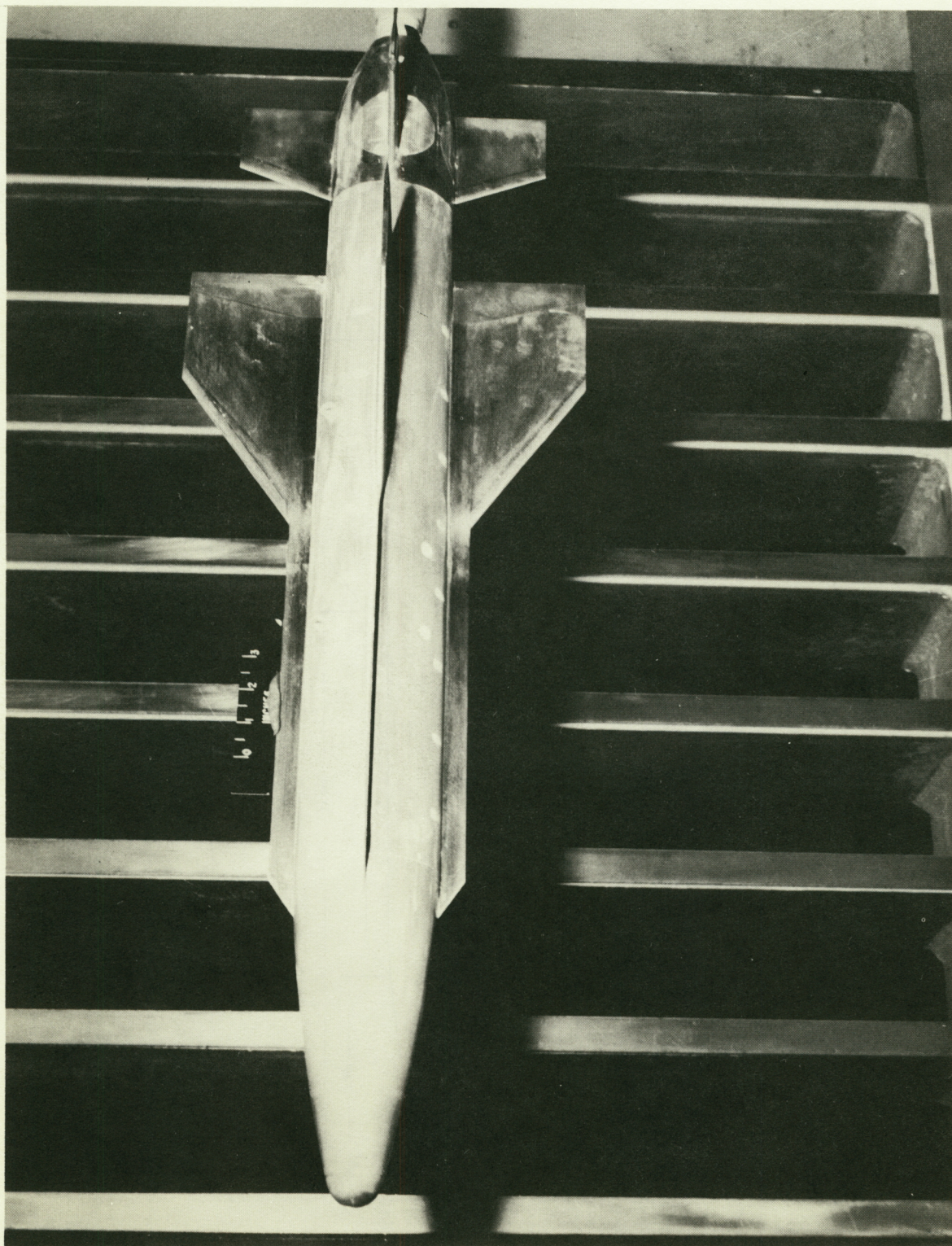
Figure 2.- Photograph of model mounted in test section.

L-64-6102
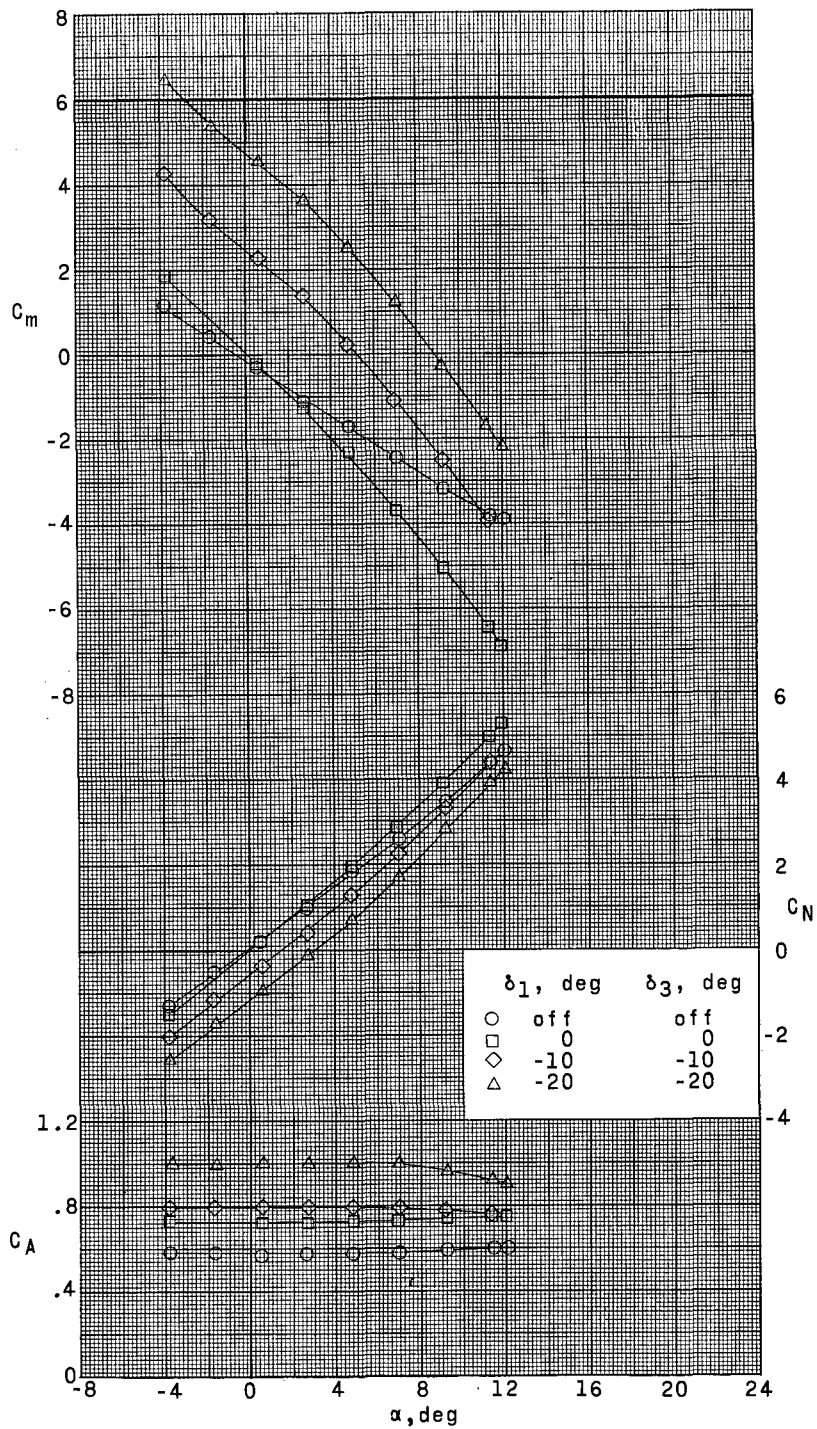
(a) M = 1.60.

Figure 3. - Effect of deflections of pitch controls on longitudinal aerodynamic characteristics. $\delta_2 = \delta_4 = 0^0$.
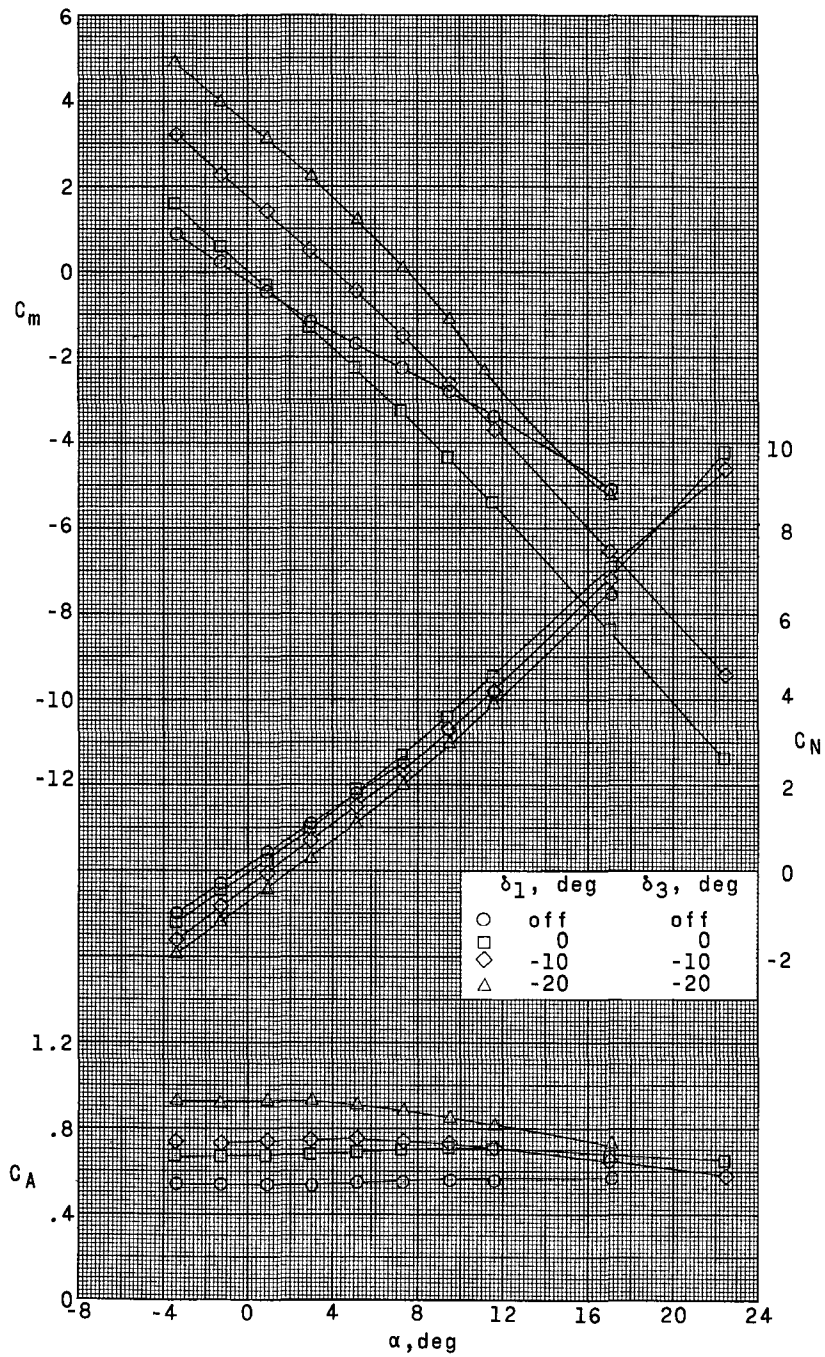
(b) M = 2.00.
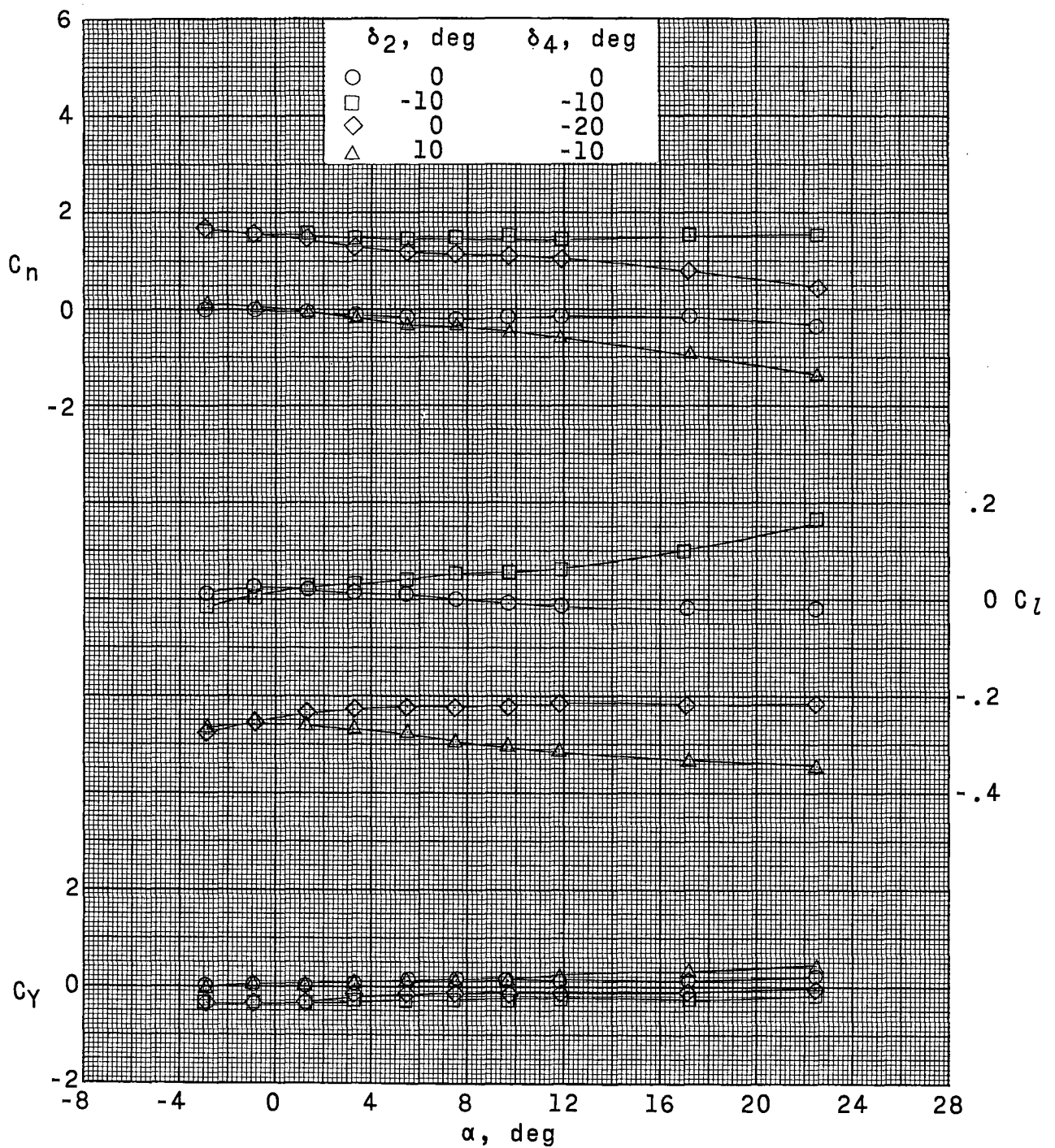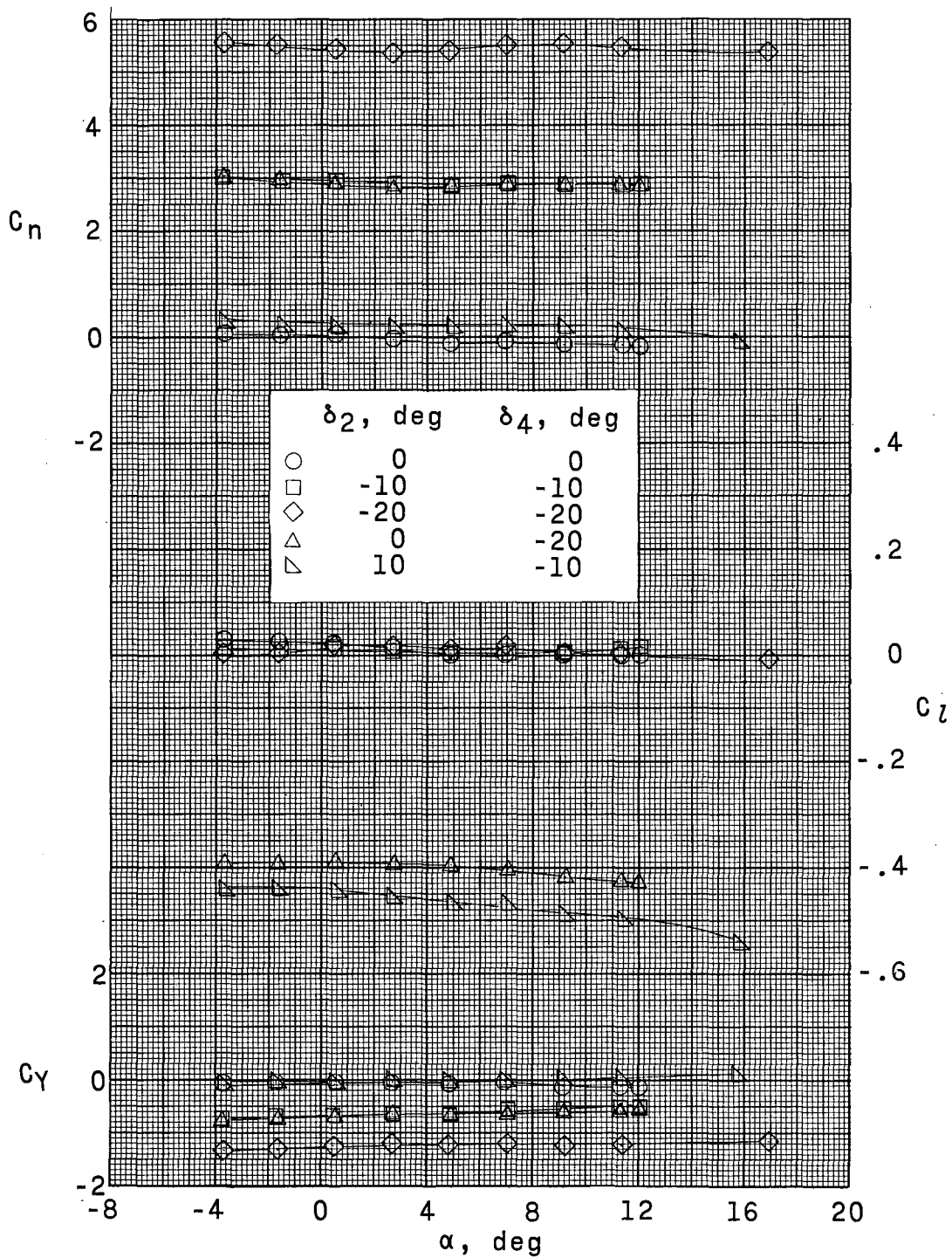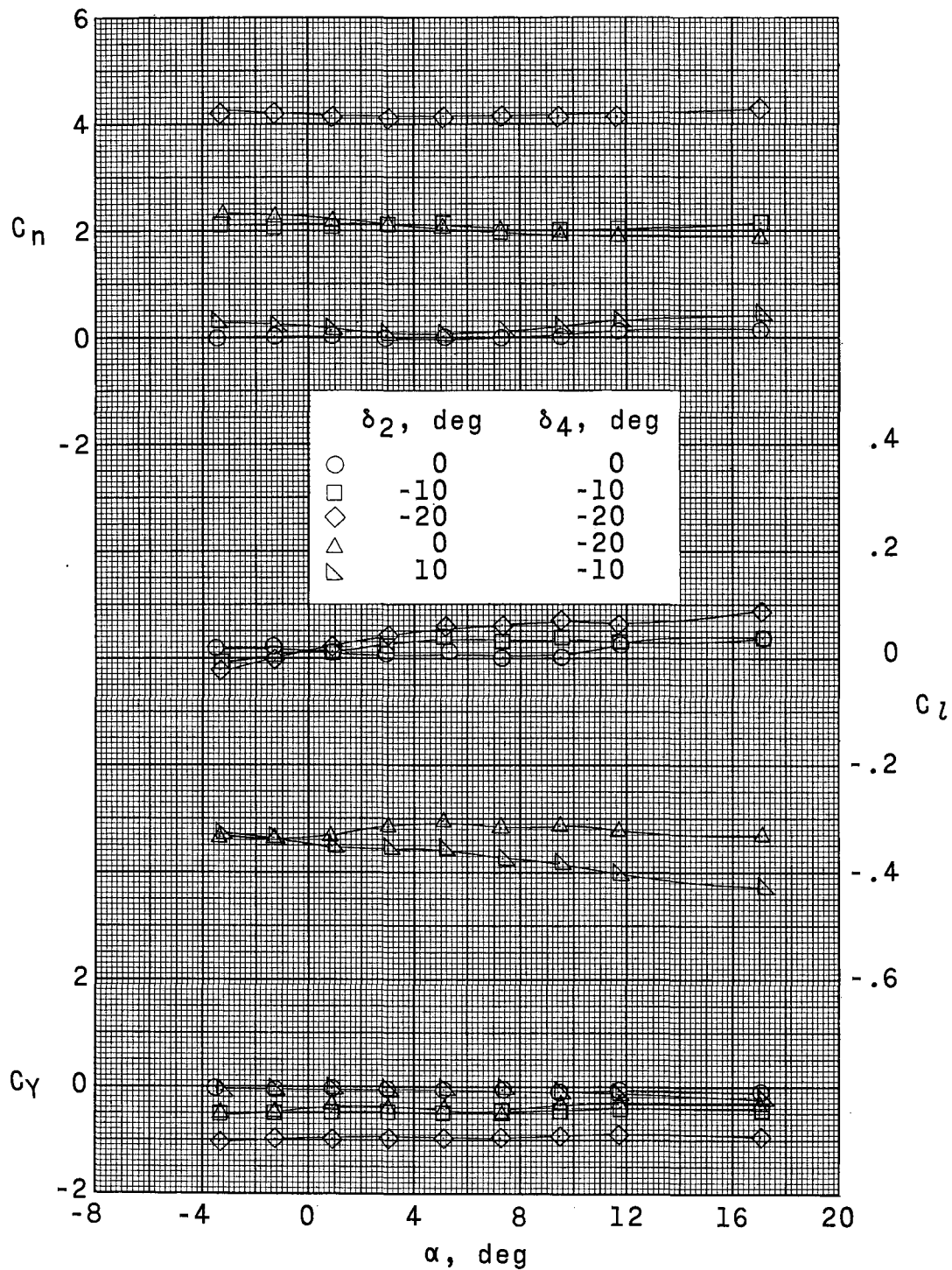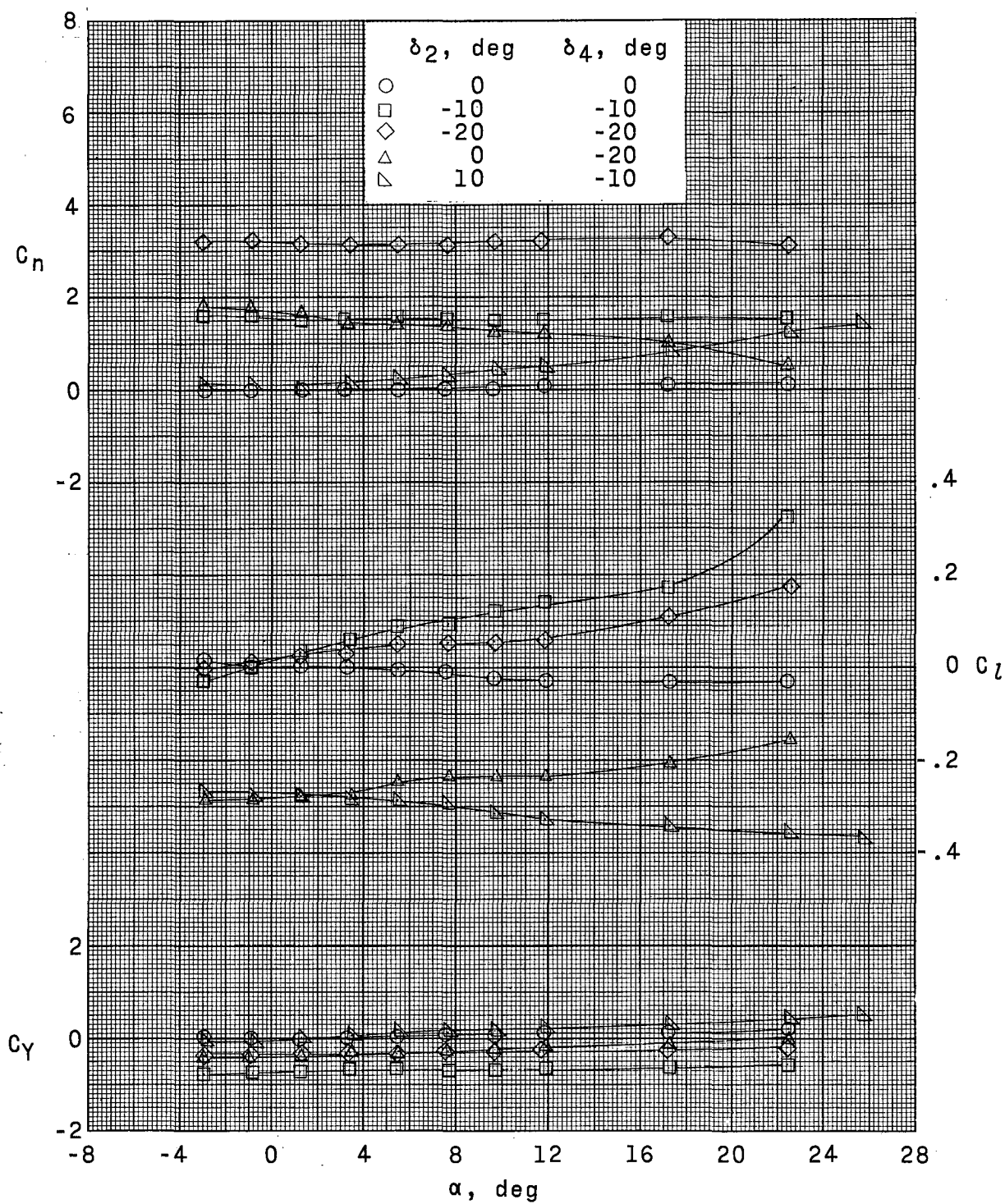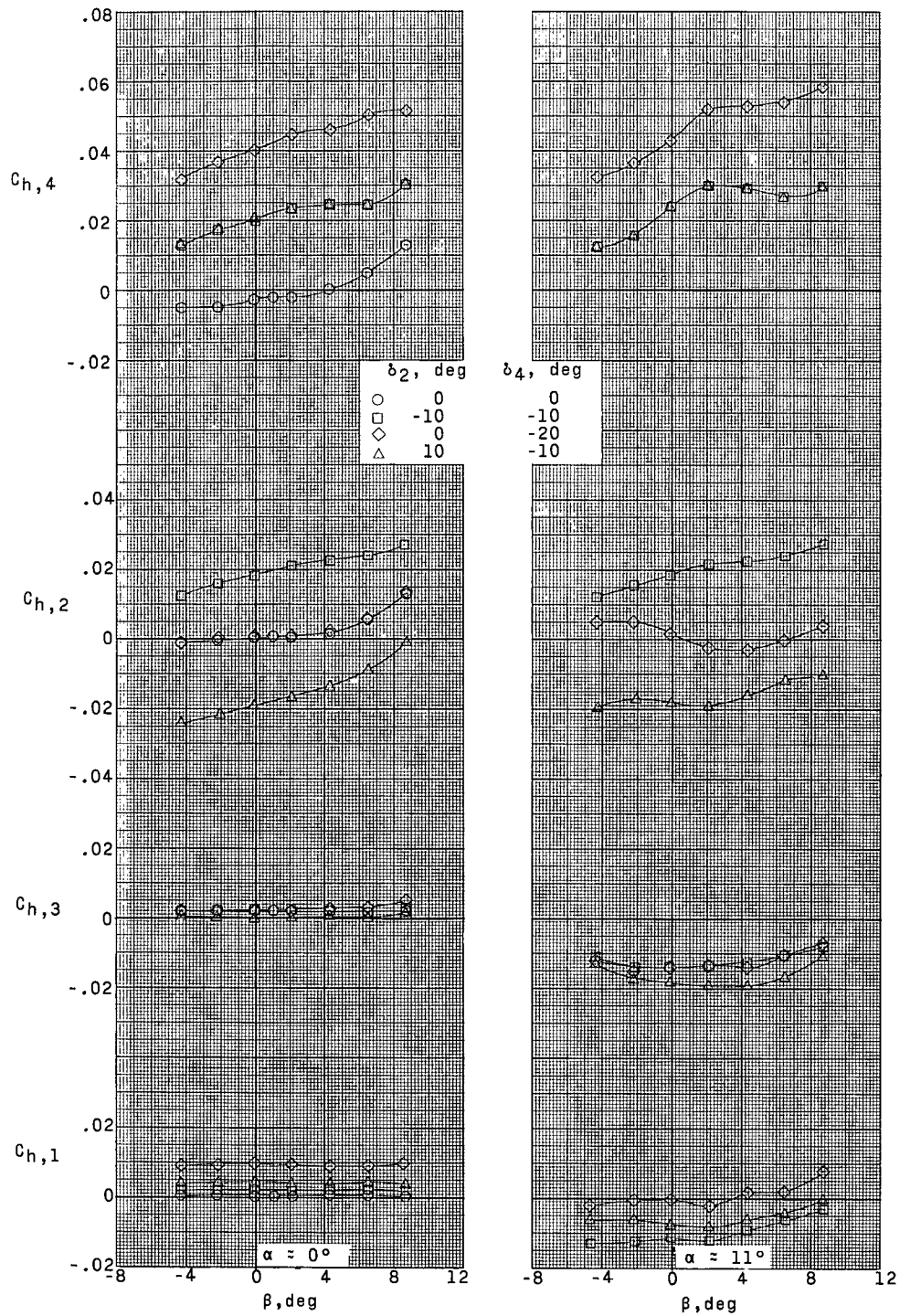
Figure 3.– Continued.
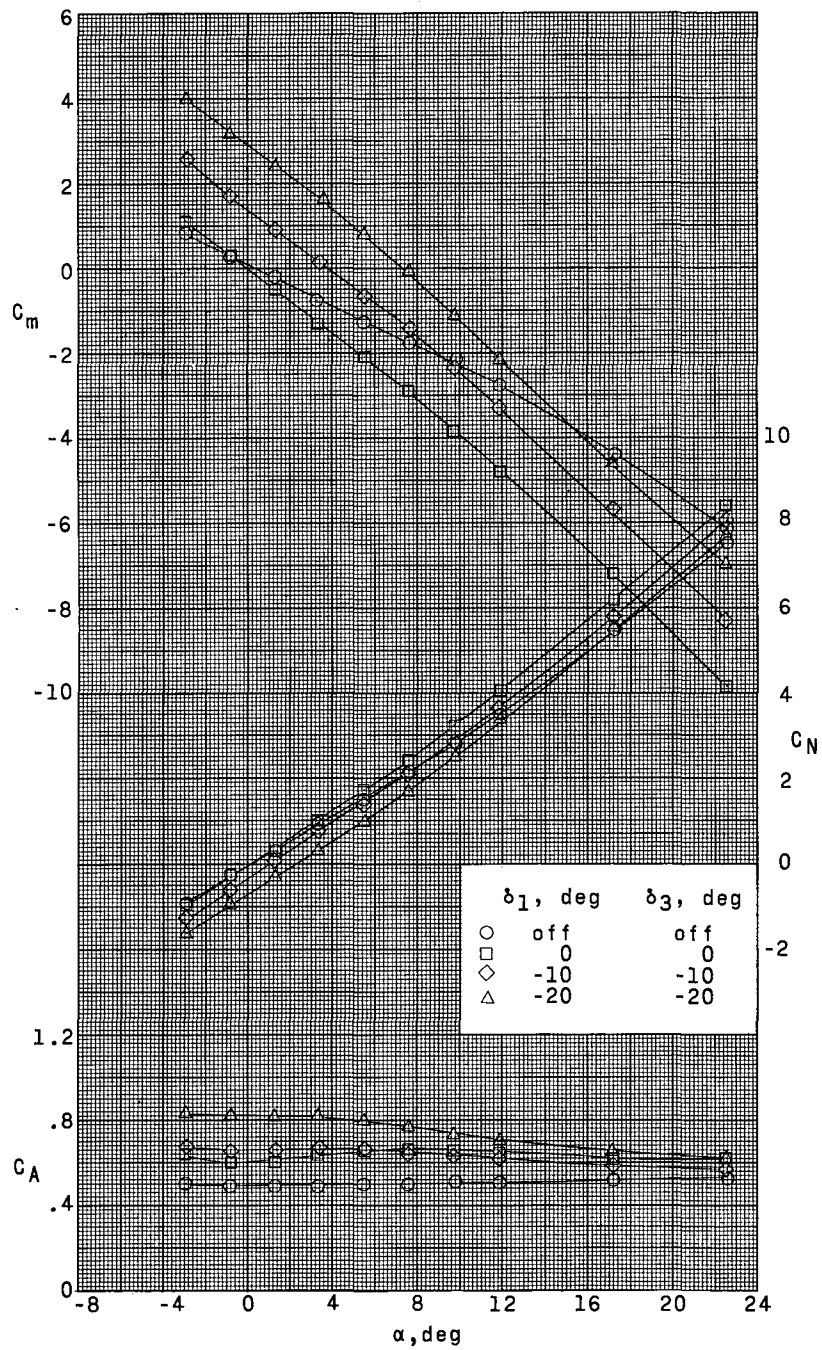
(c) M = 2.50.

Figure 3. - Concluded.
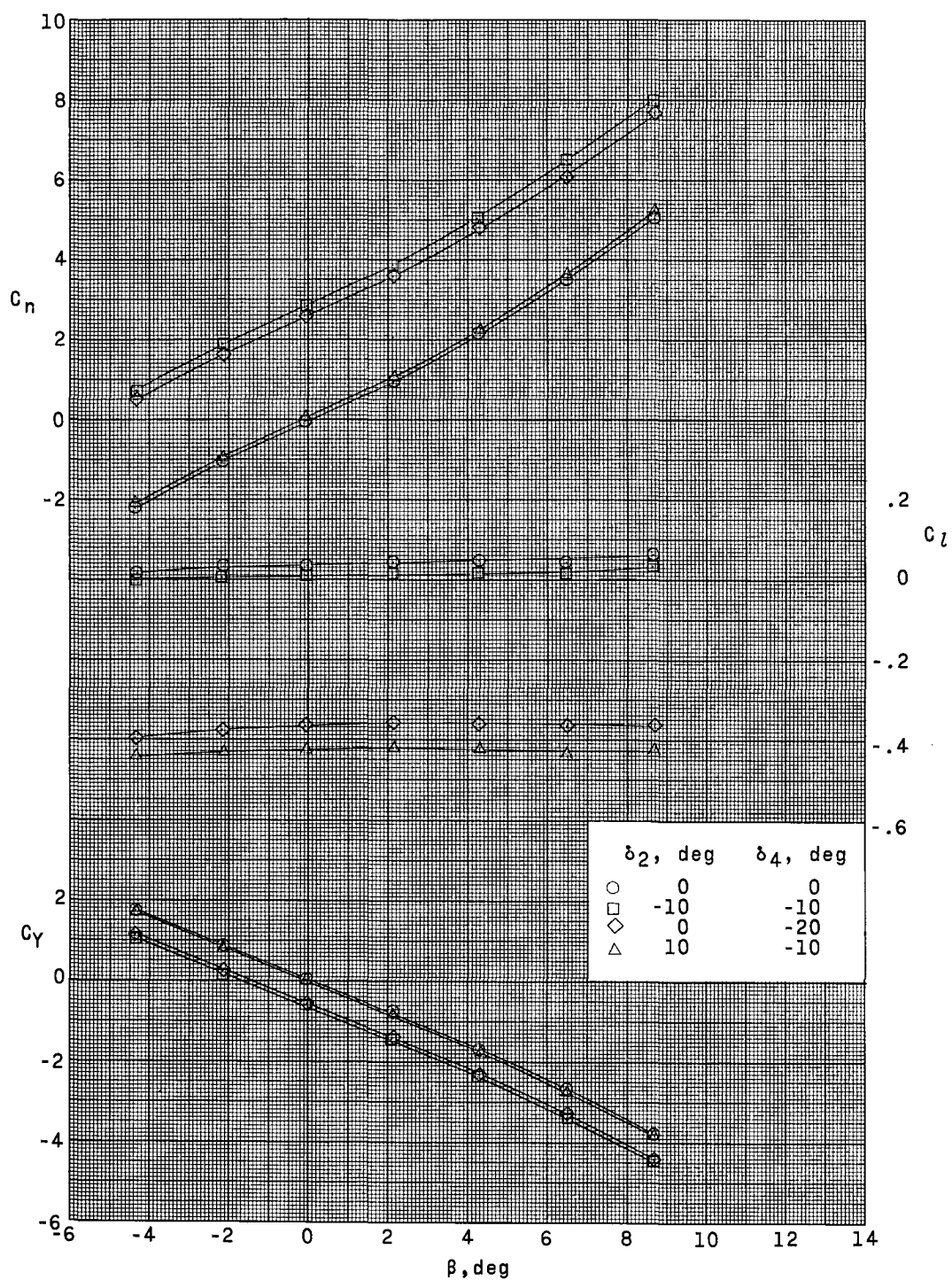
(a) M = 1.60; α ≈ 0°.

Figure 4. - Effect of symmetrical and differential deflections of directional controls on aerodynamic characteristics in sideslip. $\delta_1 = \delta_3 = 0°$.

(b) M = 1.60; α ≈ 11⁰.
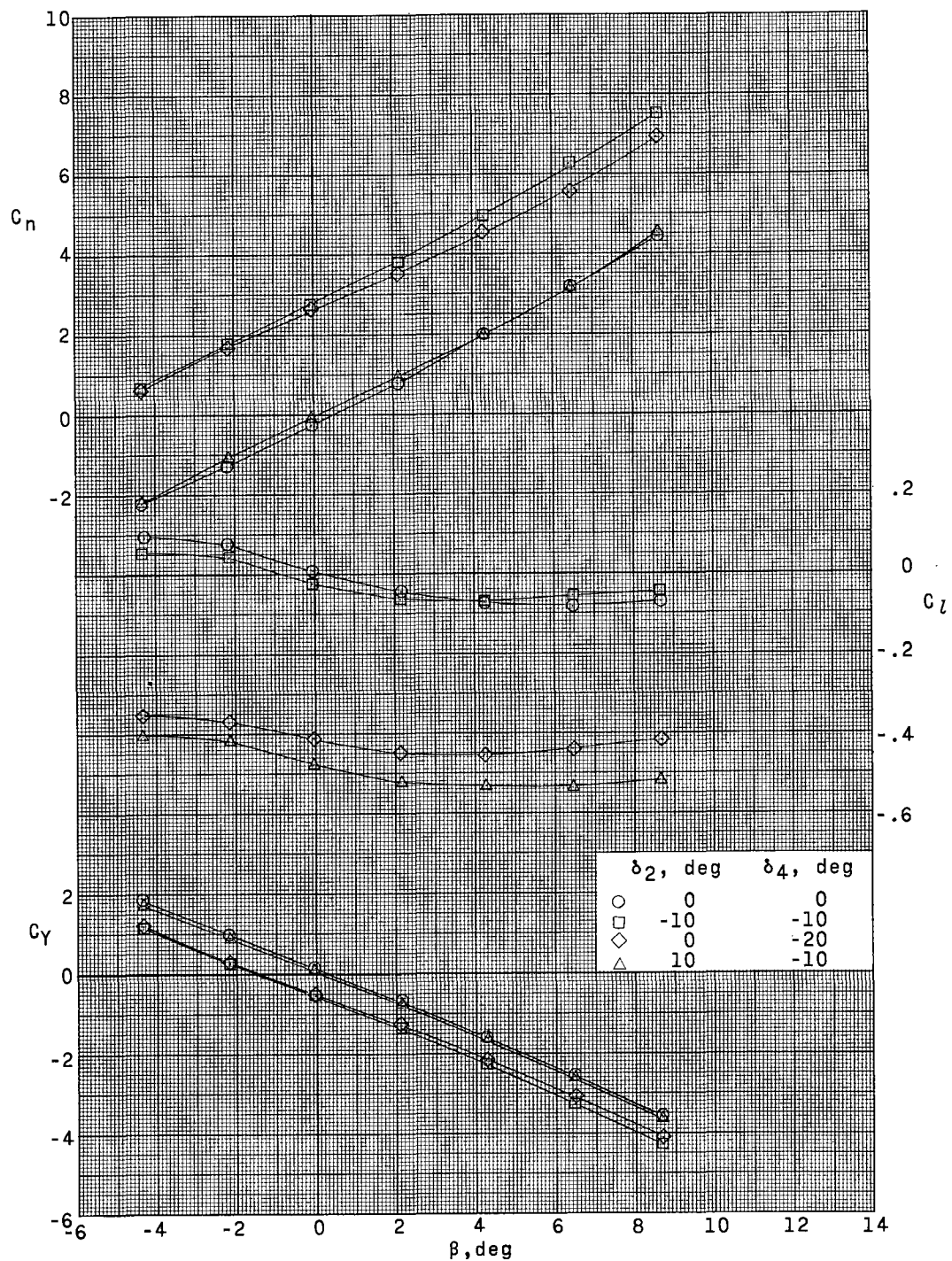
Figure 4. - Continued.

(c) M = 2.00; α ≈ 0°.
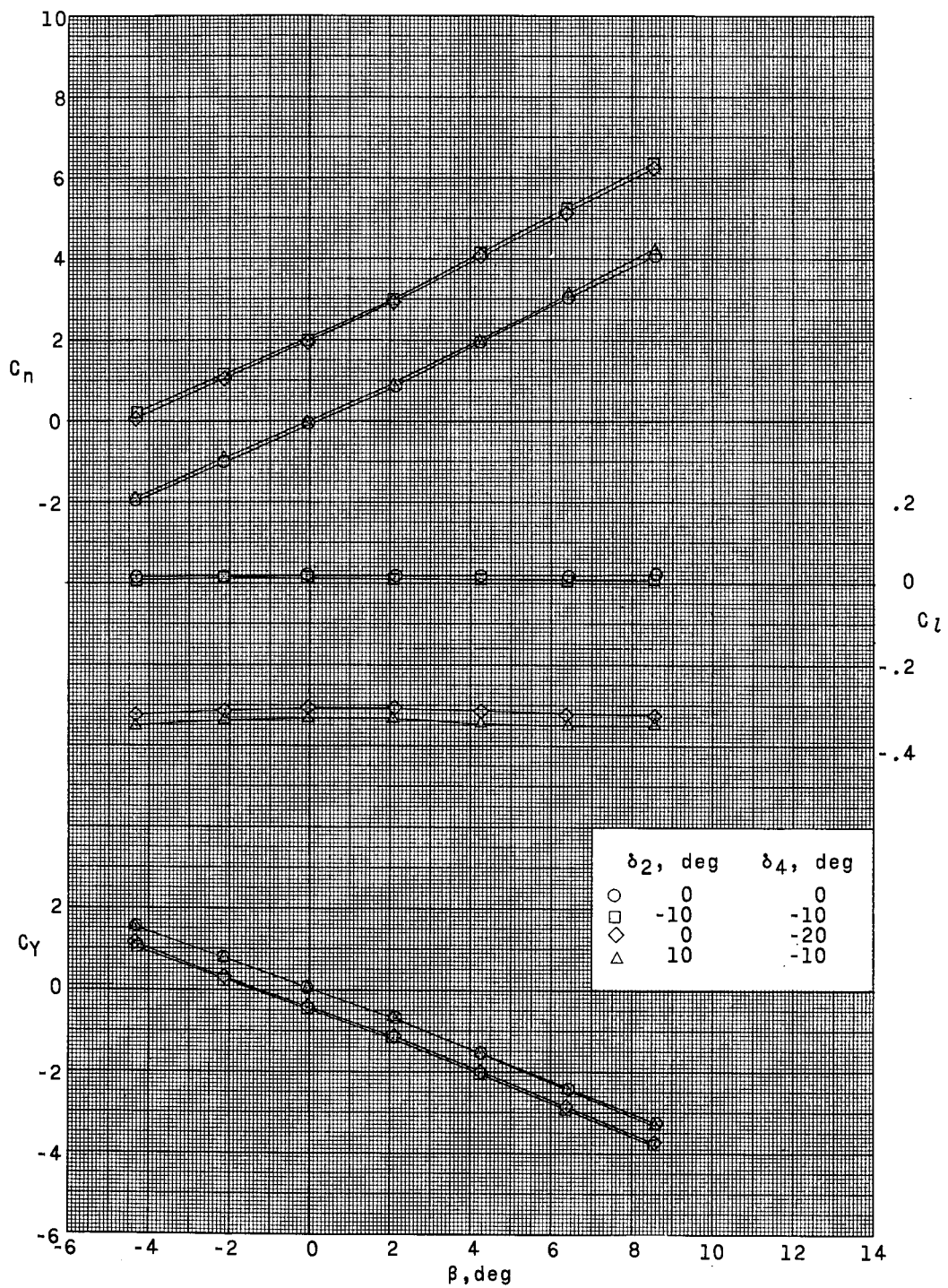
Figure 4. - Continued.
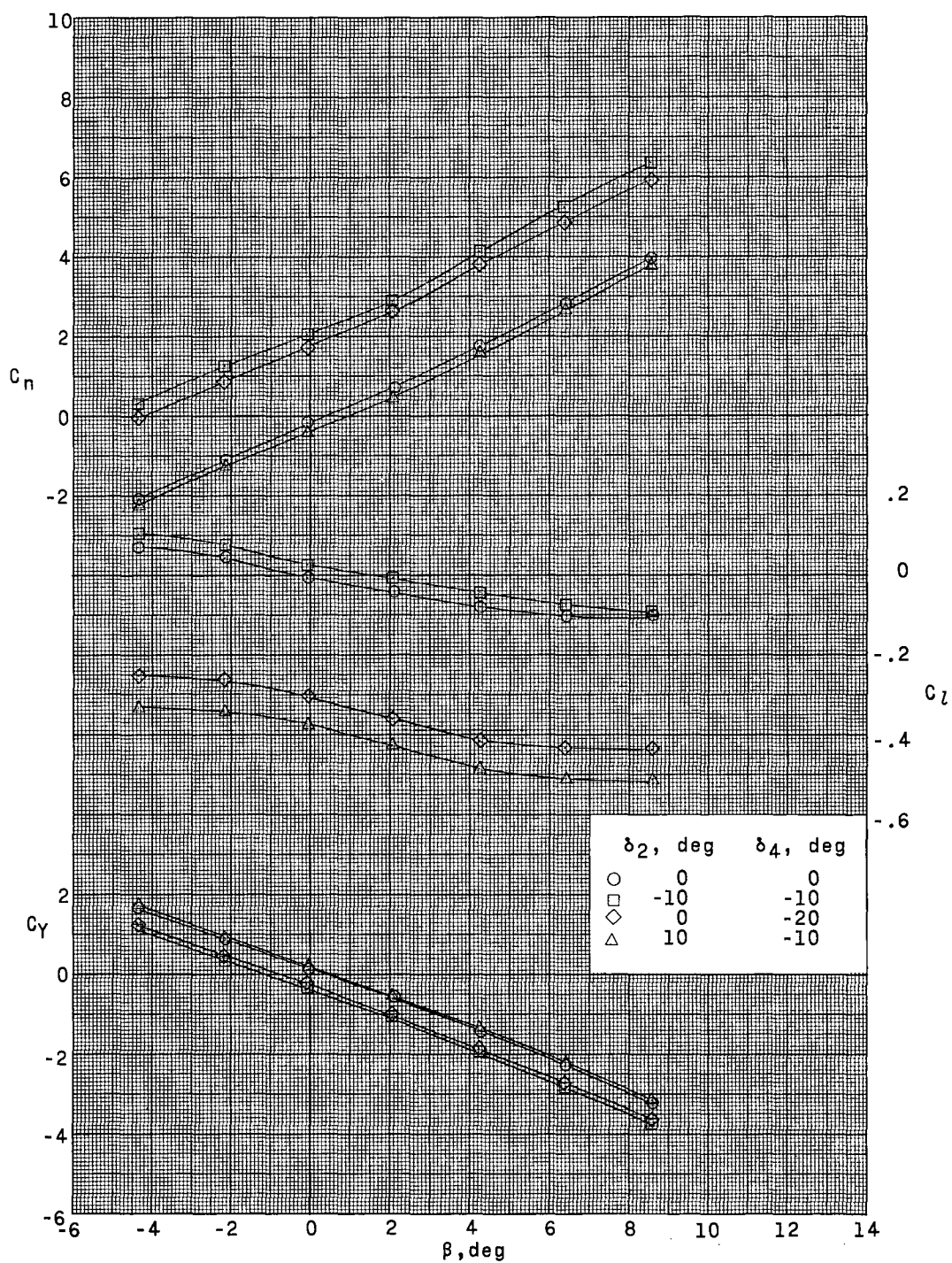
(d) M = 2.00; α ≈ 11°.

Figure 4. - Continued.
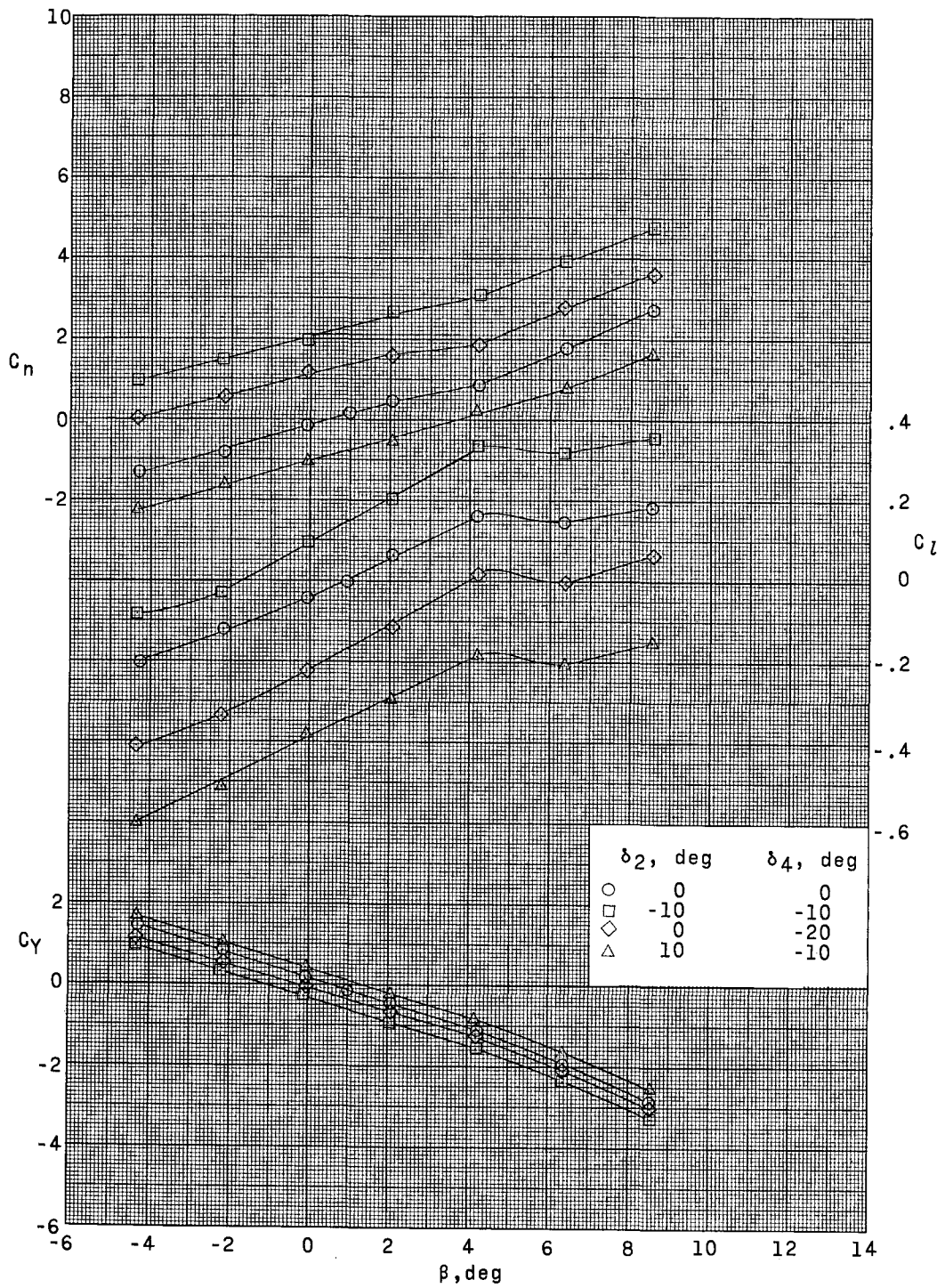
(e) M = 2.00; α ≈ 22°.

Figure 4. - Continued.
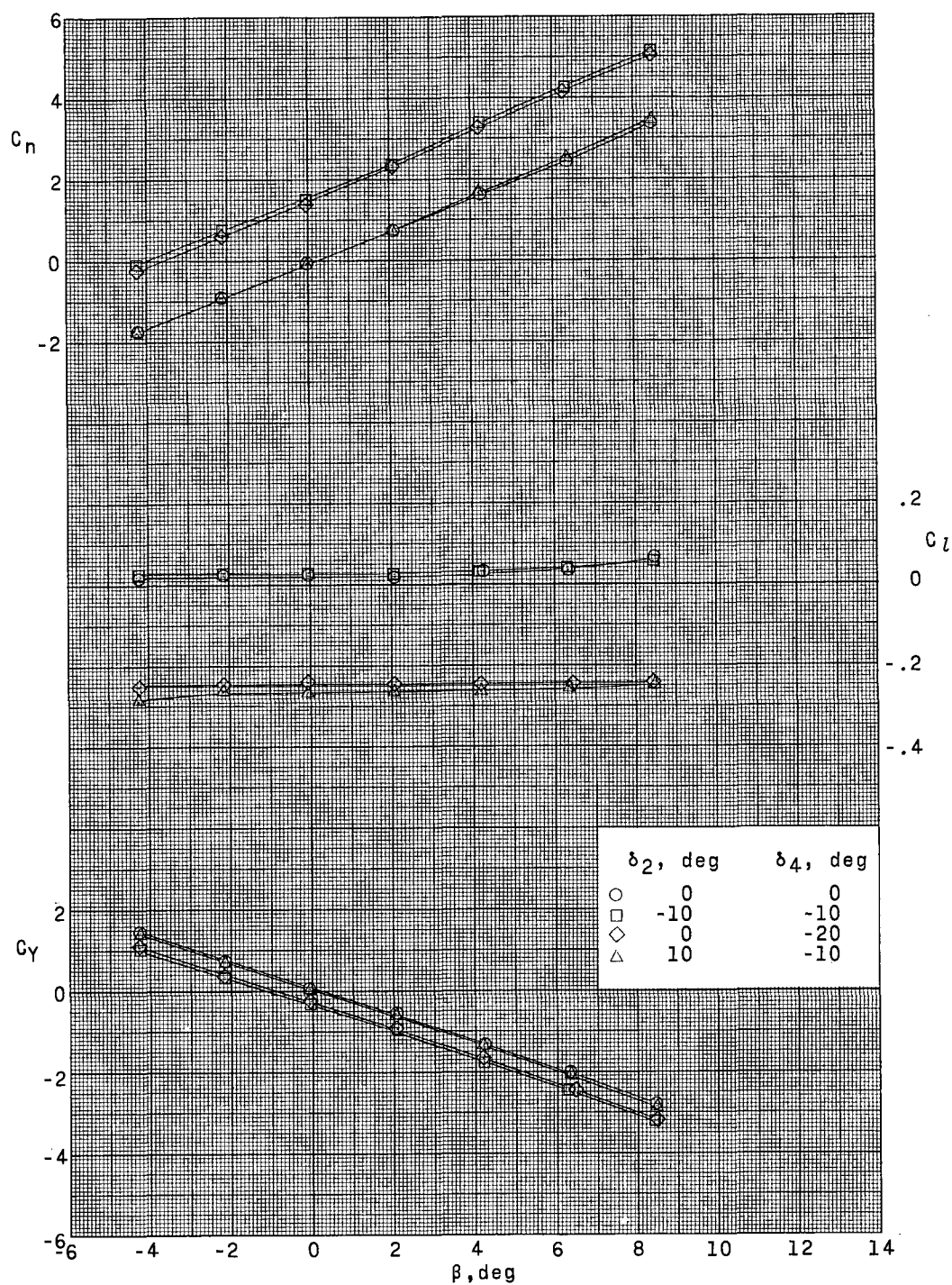
(f) M = 2.50; α ≈ 0⁰.

Figure 4. - Continued.

(g) M = 2.50; α ≈ 11⁰.
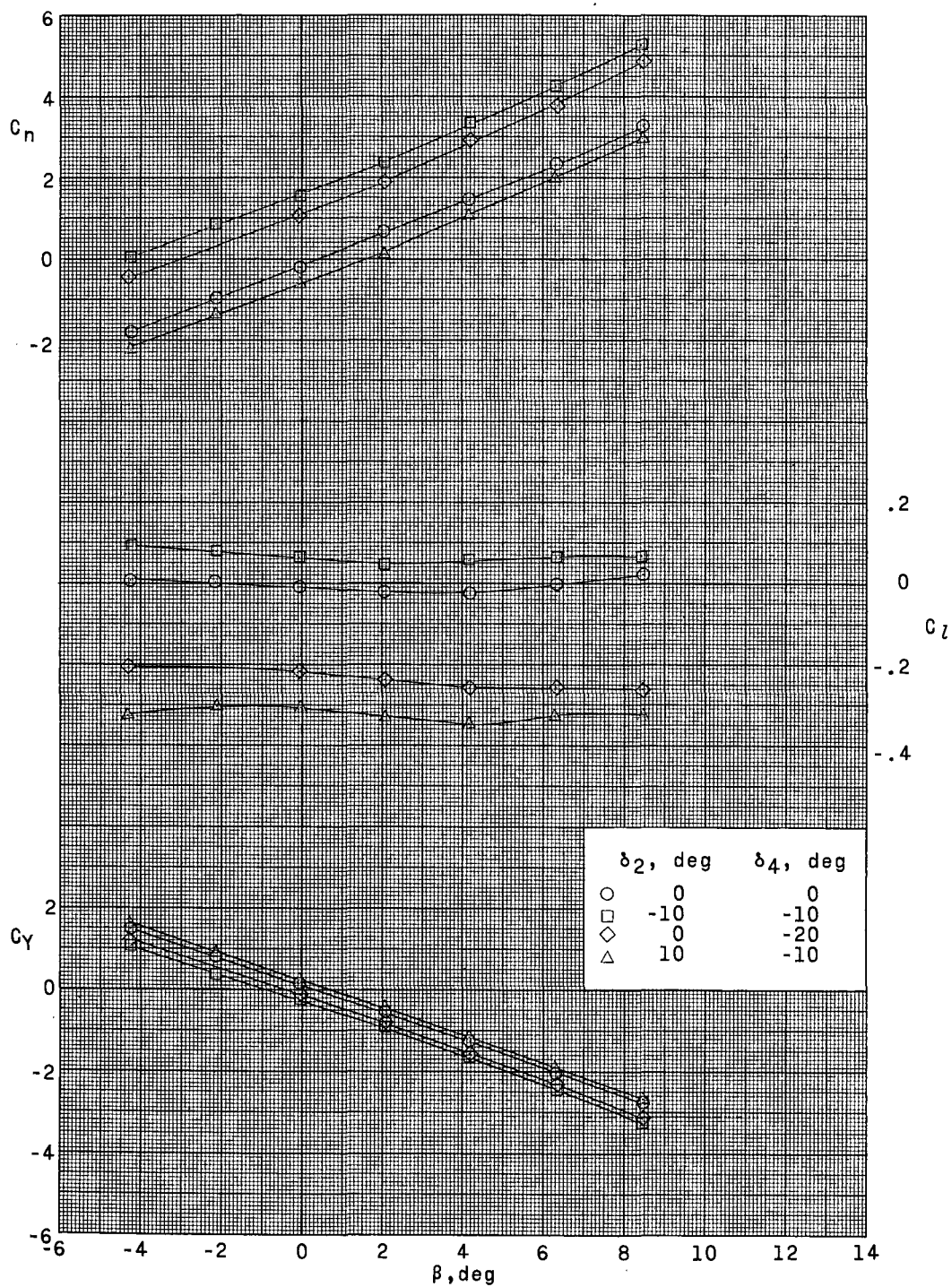
Figure 4. - Continued.

(h) M = 2.50; α ≈ 22⁰.
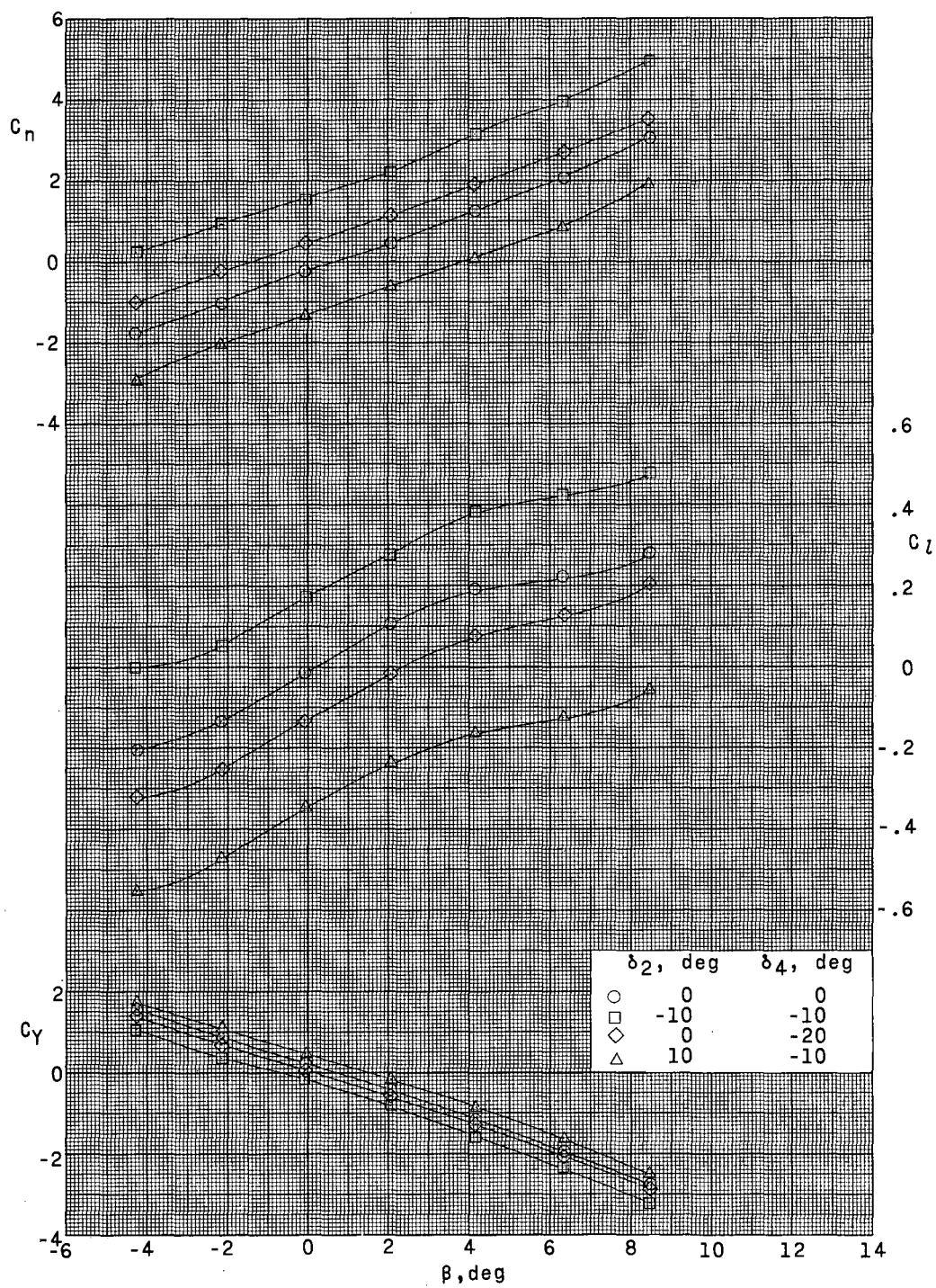
Figure 4. - Concluded.
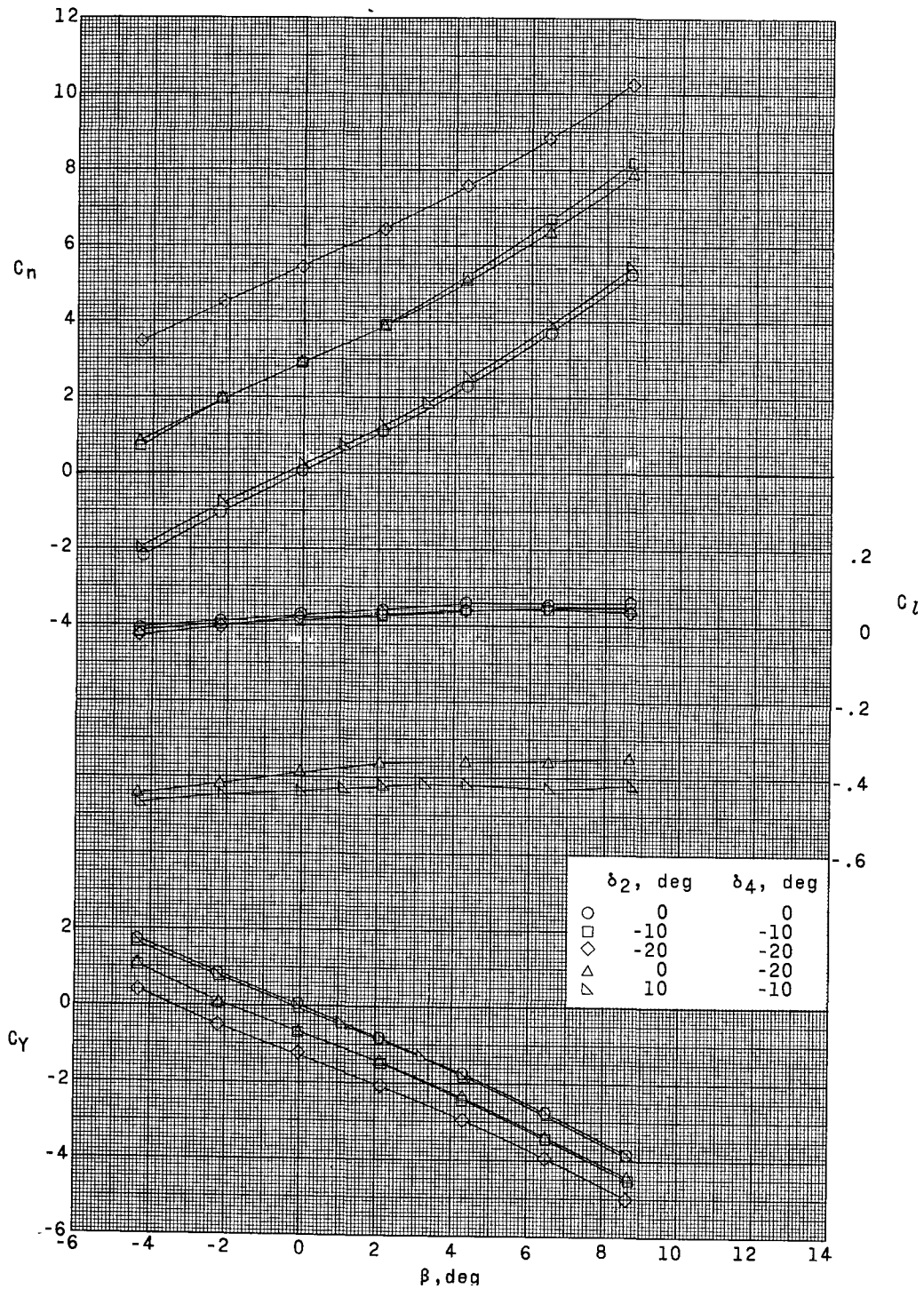
(a) M = 1.60; $\alpha \approx 0°$.

Figure 5. – Effect of symmetrical and differential deflections of directional controls on aerodynamic characteristics in sideslip. $\delta_1 = \delta_3 = -20°$.

(b) M = 1.60; α ≈ 11°.
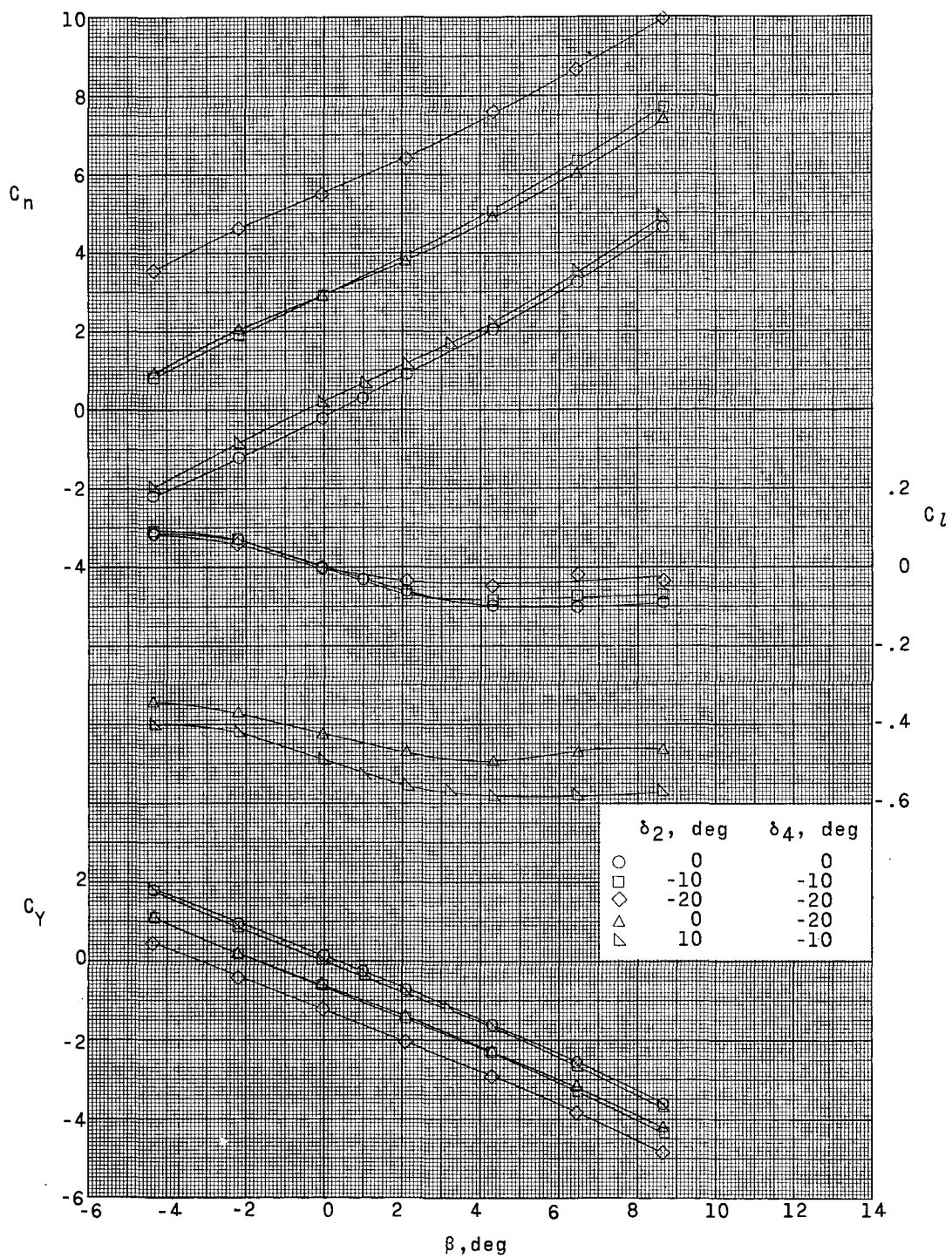
Figure 5. - Continued.

(c) M = 2.00; α ≈ 0°.
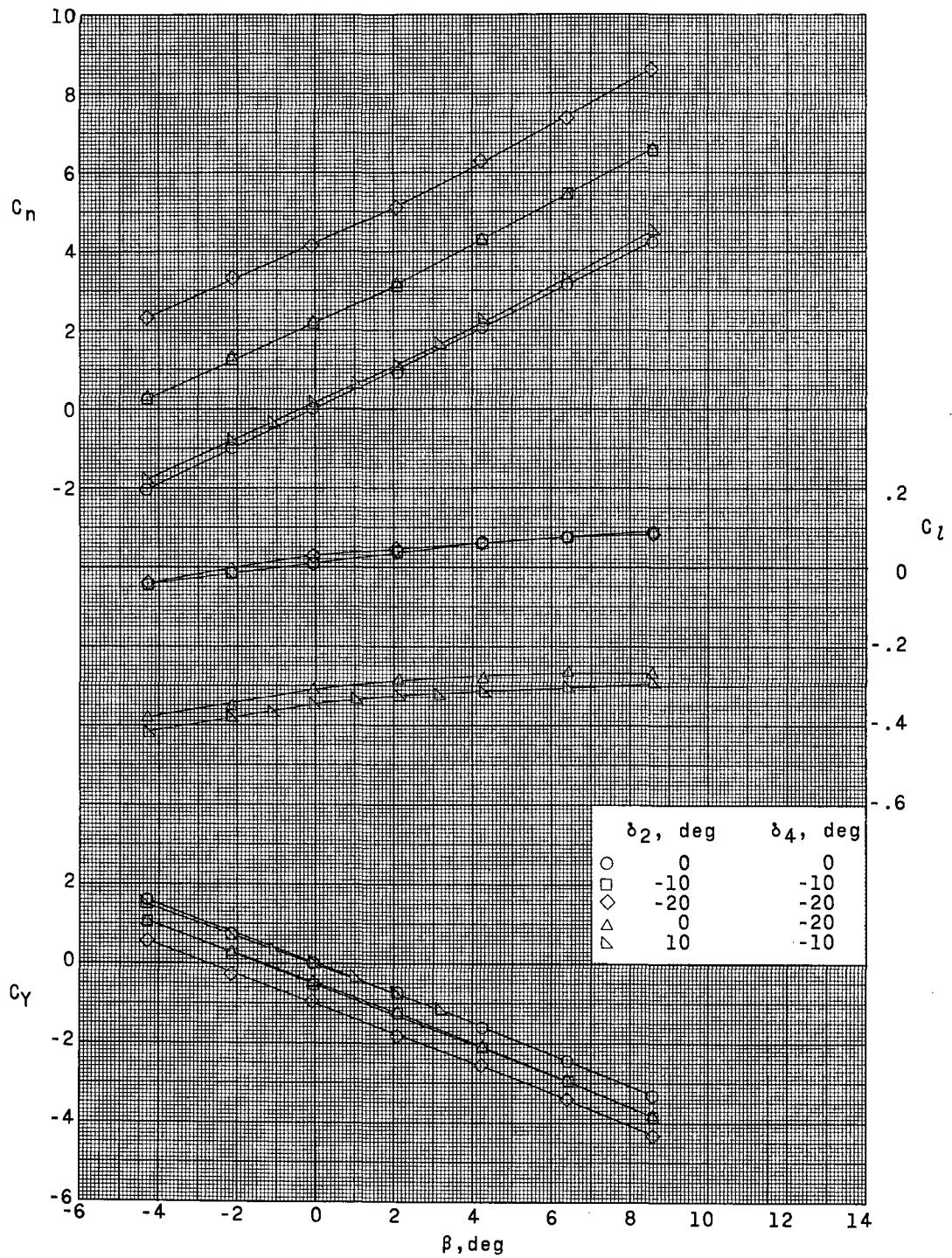
Figure 5. - Continued.

(d) M = 2.00; α ≈ 11°.
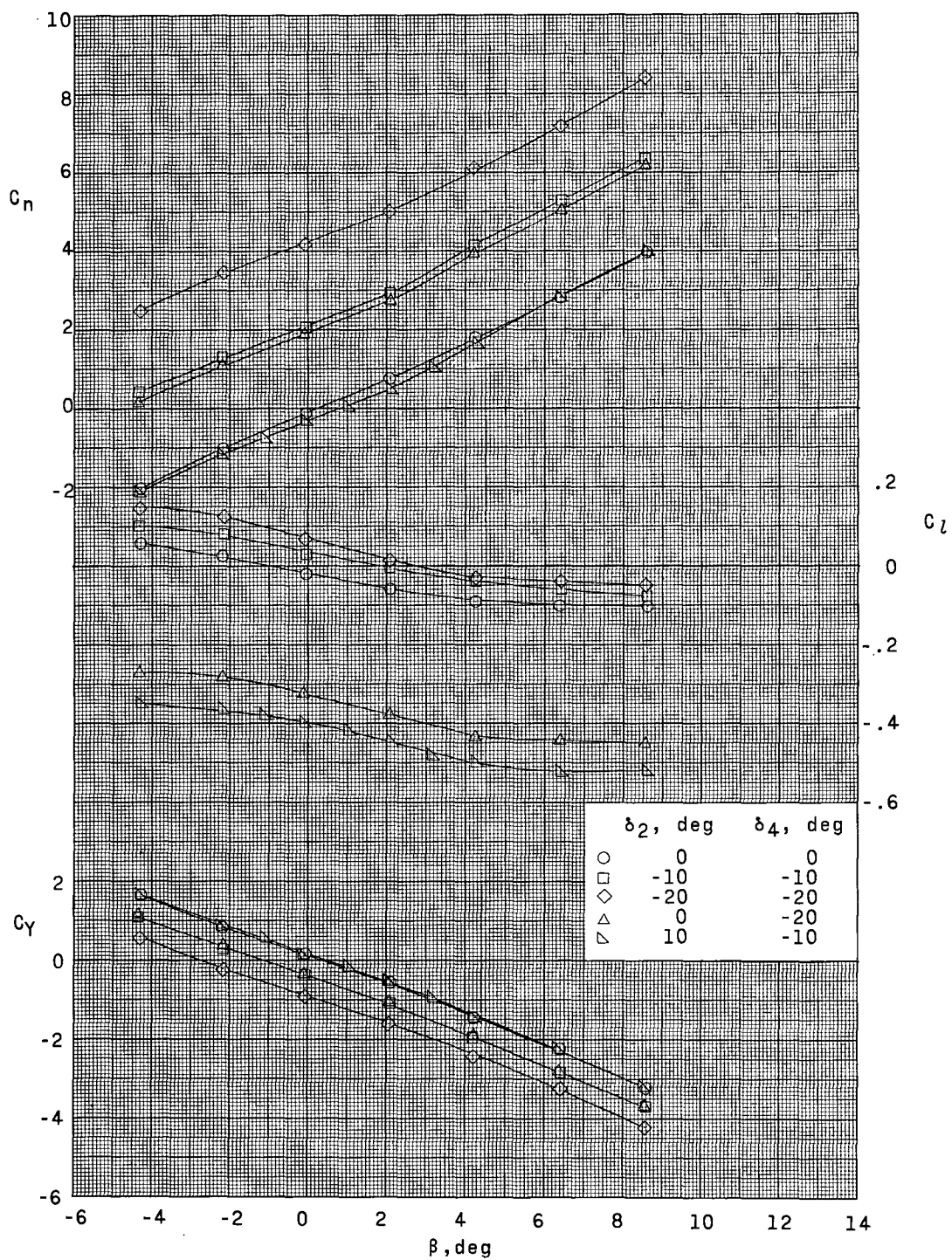
Figure 5. – Continued.

(e) M = 2.00; α ≈ 17⁰.
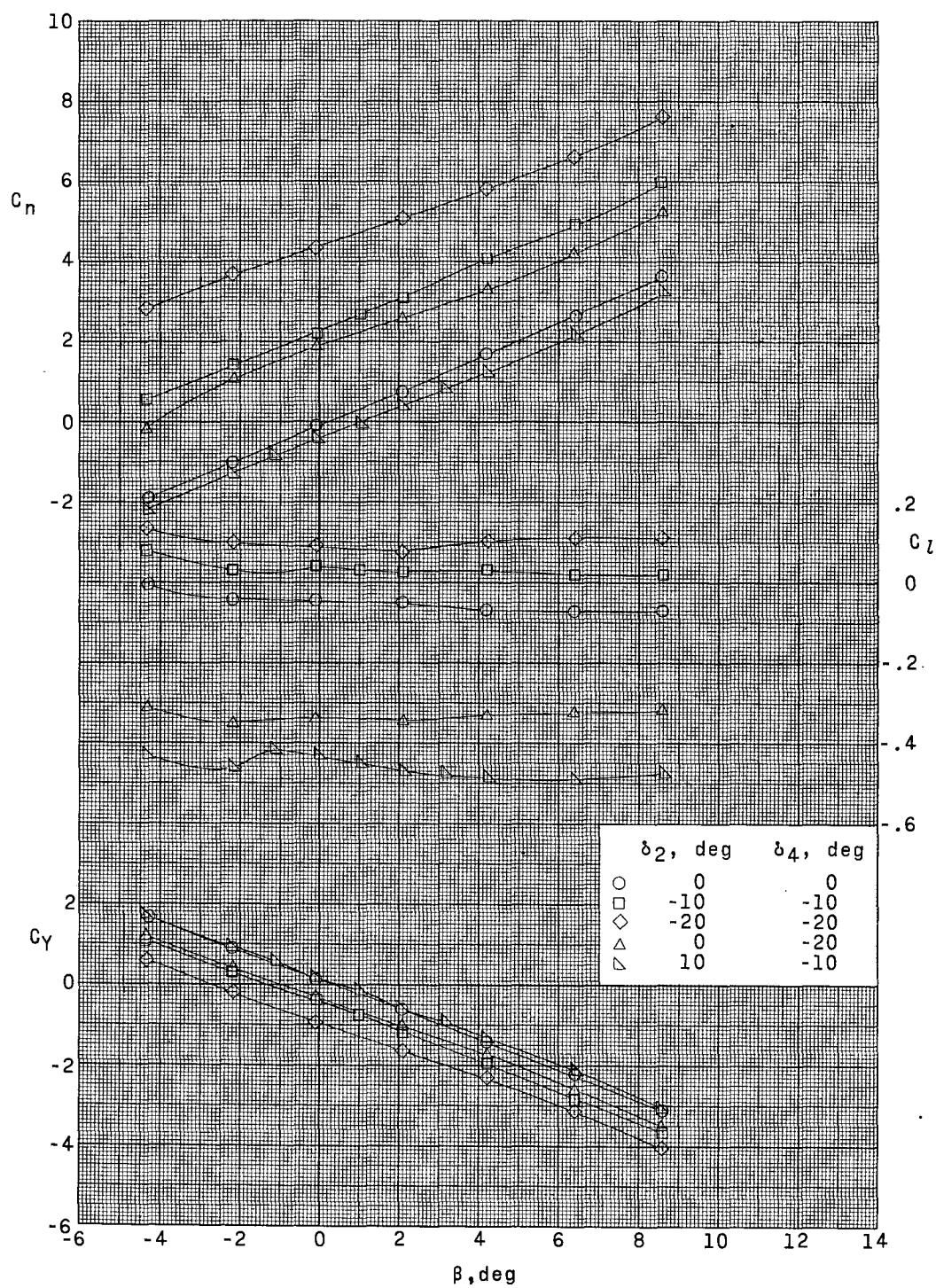
Figure 5. - Continued.
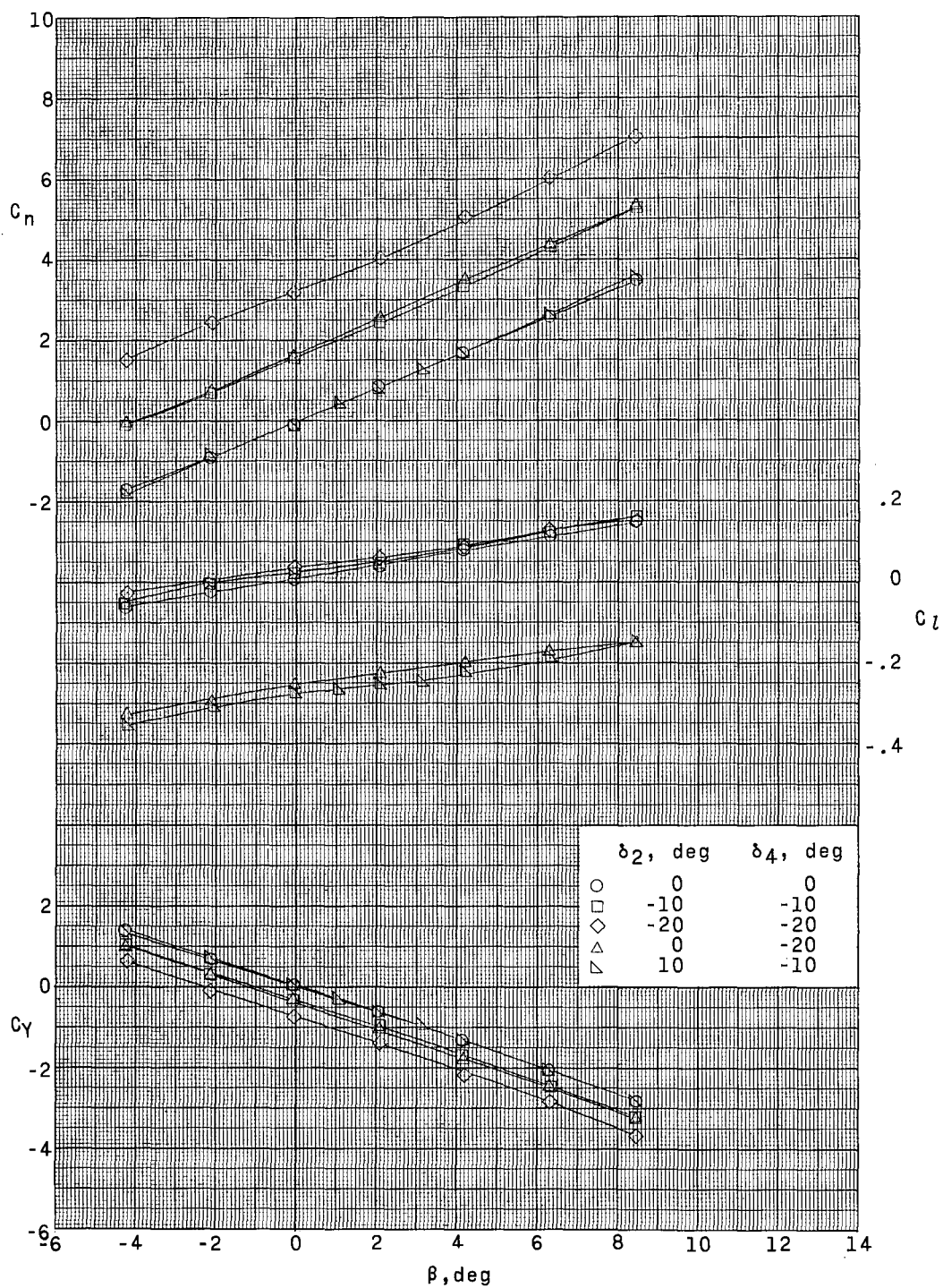
(f) M = 2.50; α ≈ 0⁰.

Figure 5. - Continued.

(g) M = 2.50; α ≈ 11⁰.
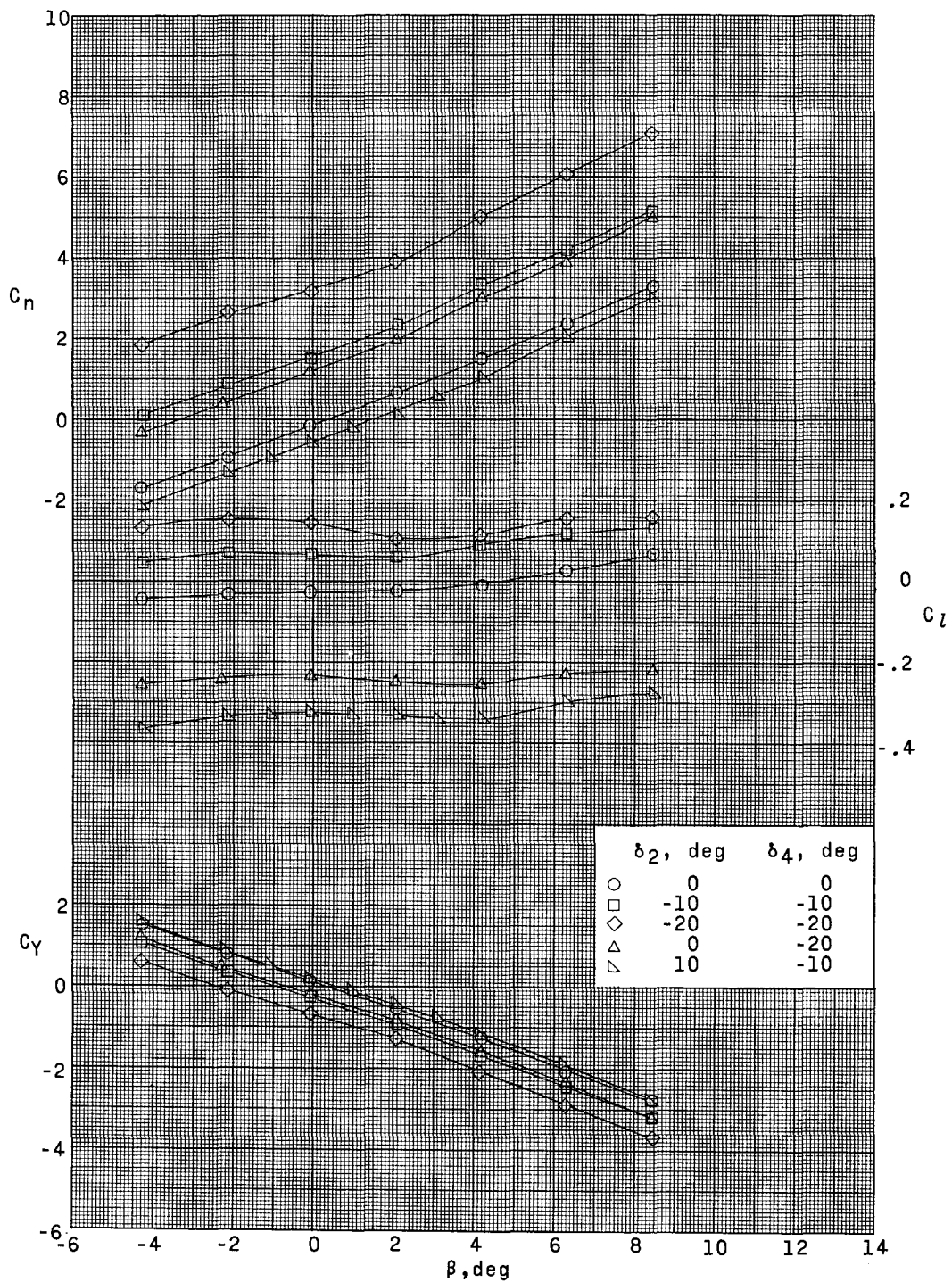
Figure 5. - Continued.
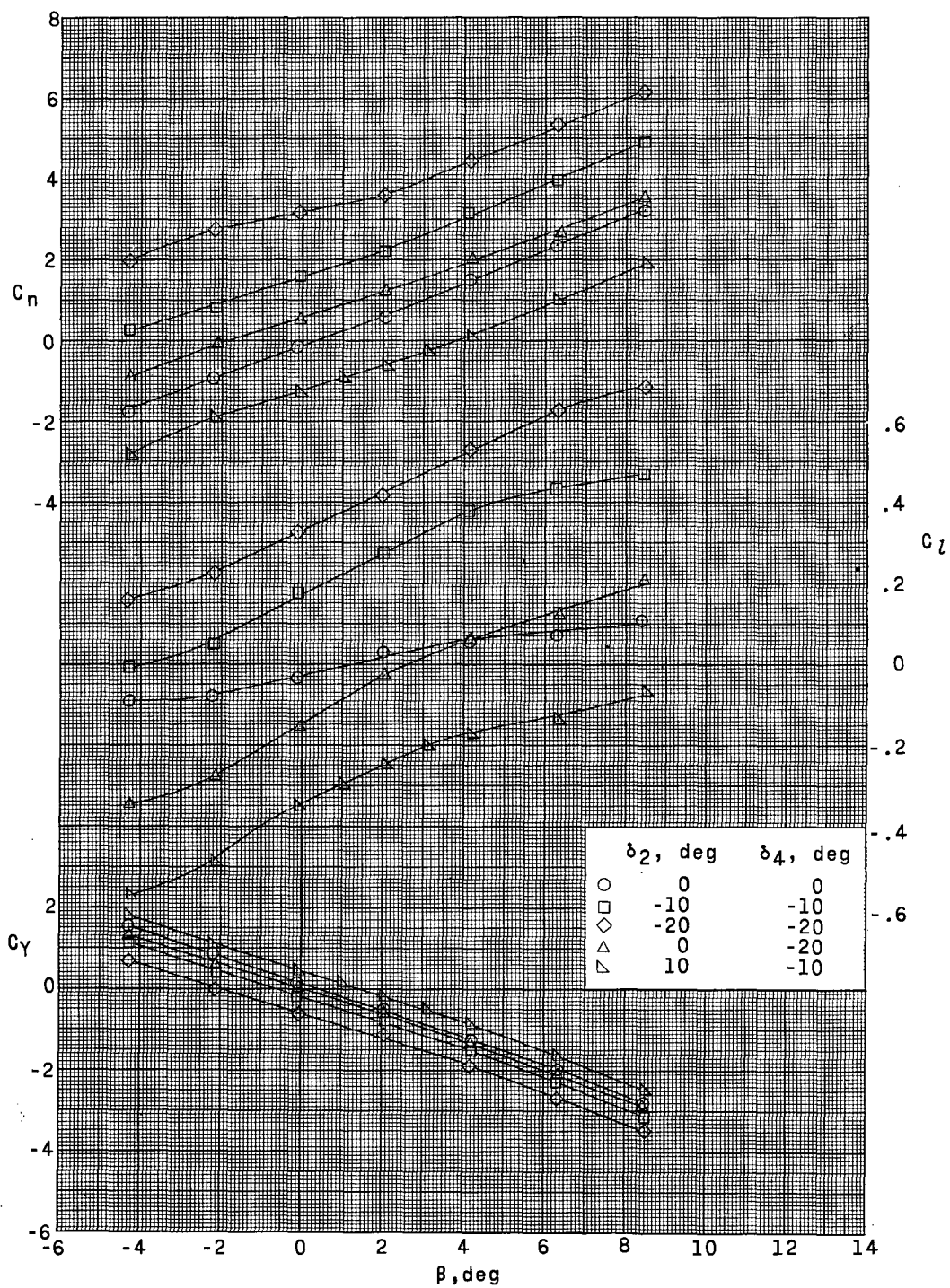
(h) M = 2.50; α ≈ 22° (with the exception of δ₂ = δ₄ = 0°, where α ≈ 17°).

Figure 5.- Concluded.
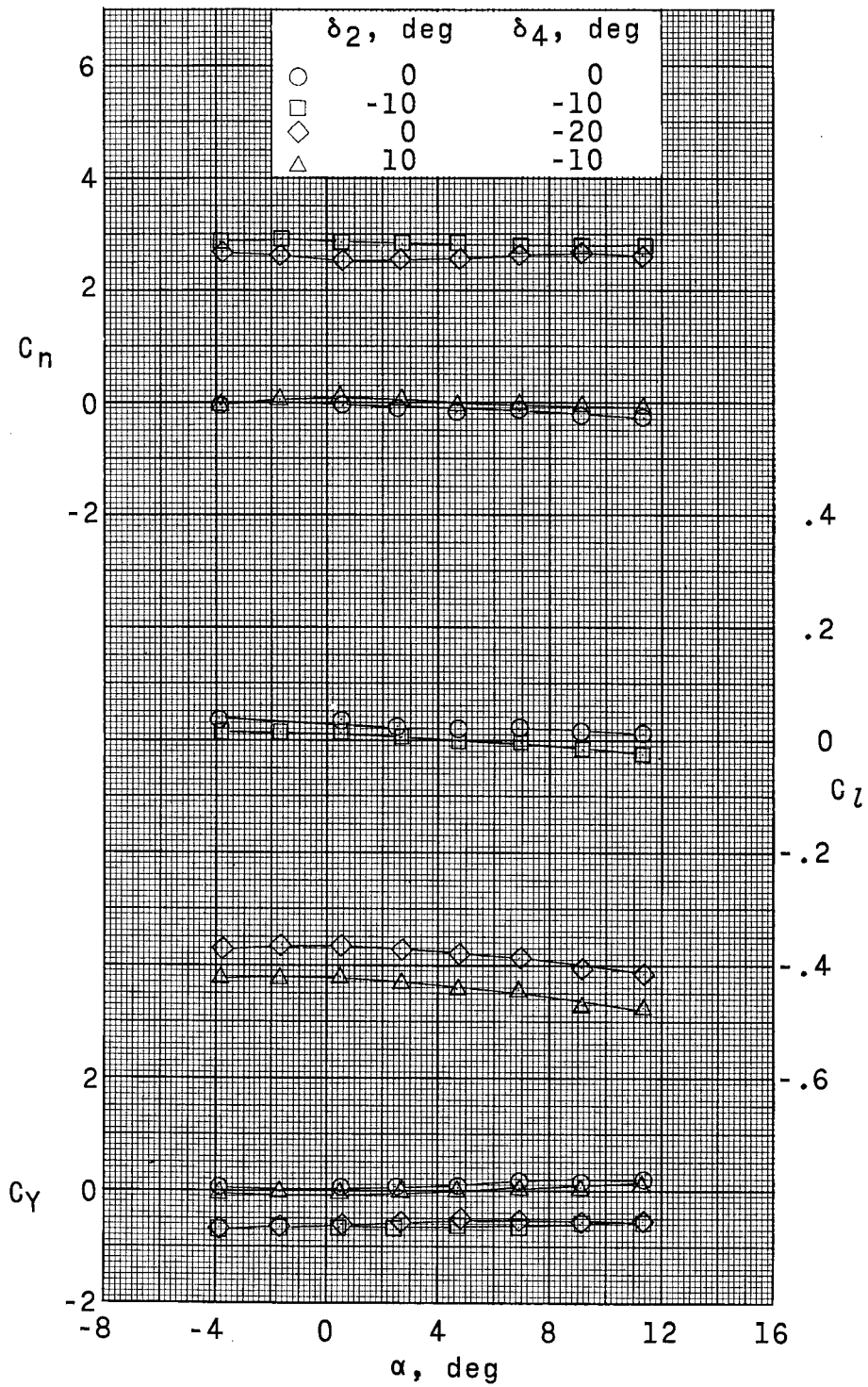
(a) M = 1.60.

Figure 6. - Effect of symmetrical and differential deflections of directional controls on lateral aerodynamic characteristics $\delta_1 = \delta_3 = 0^o$; $\beta = 0^o$.
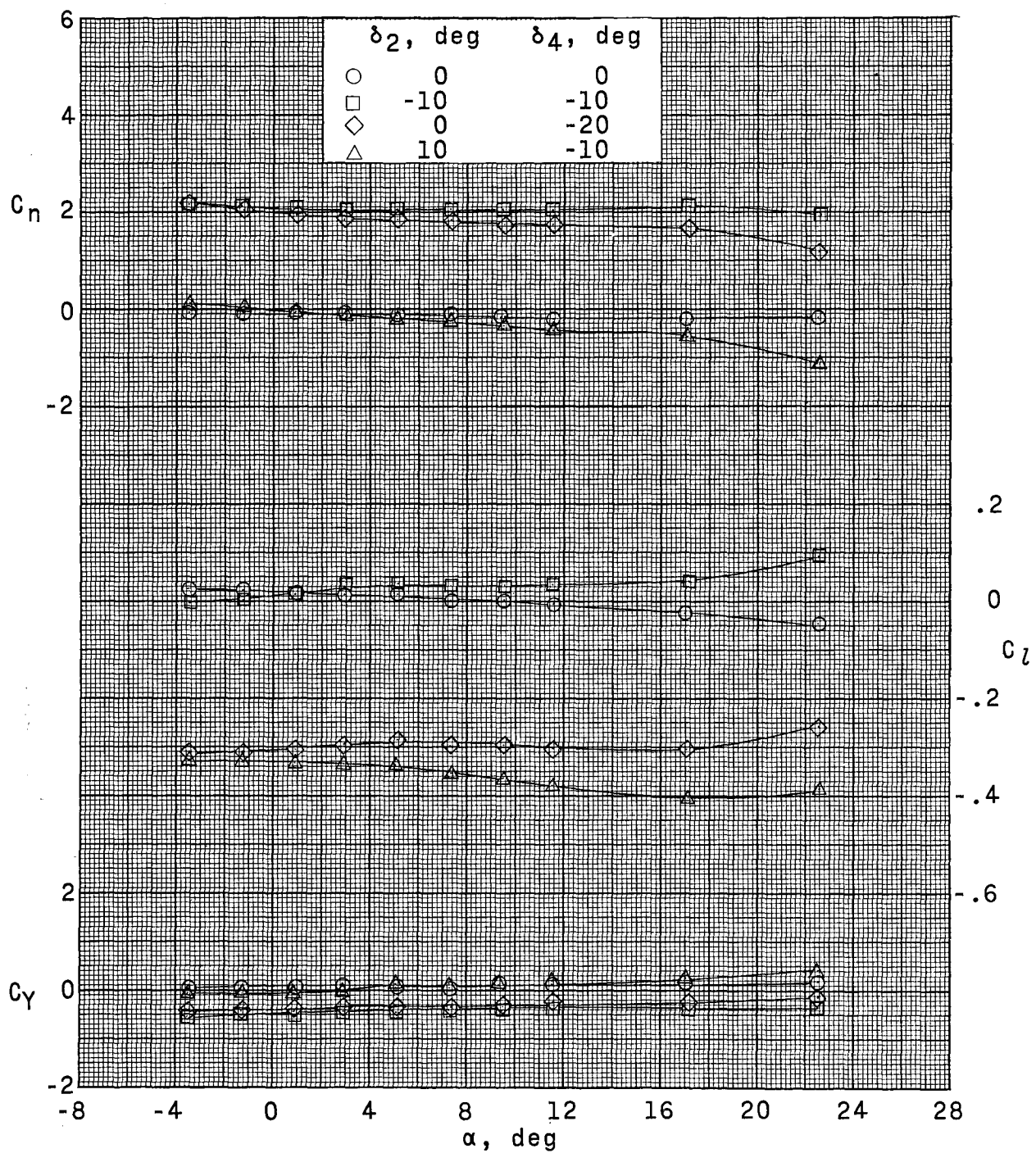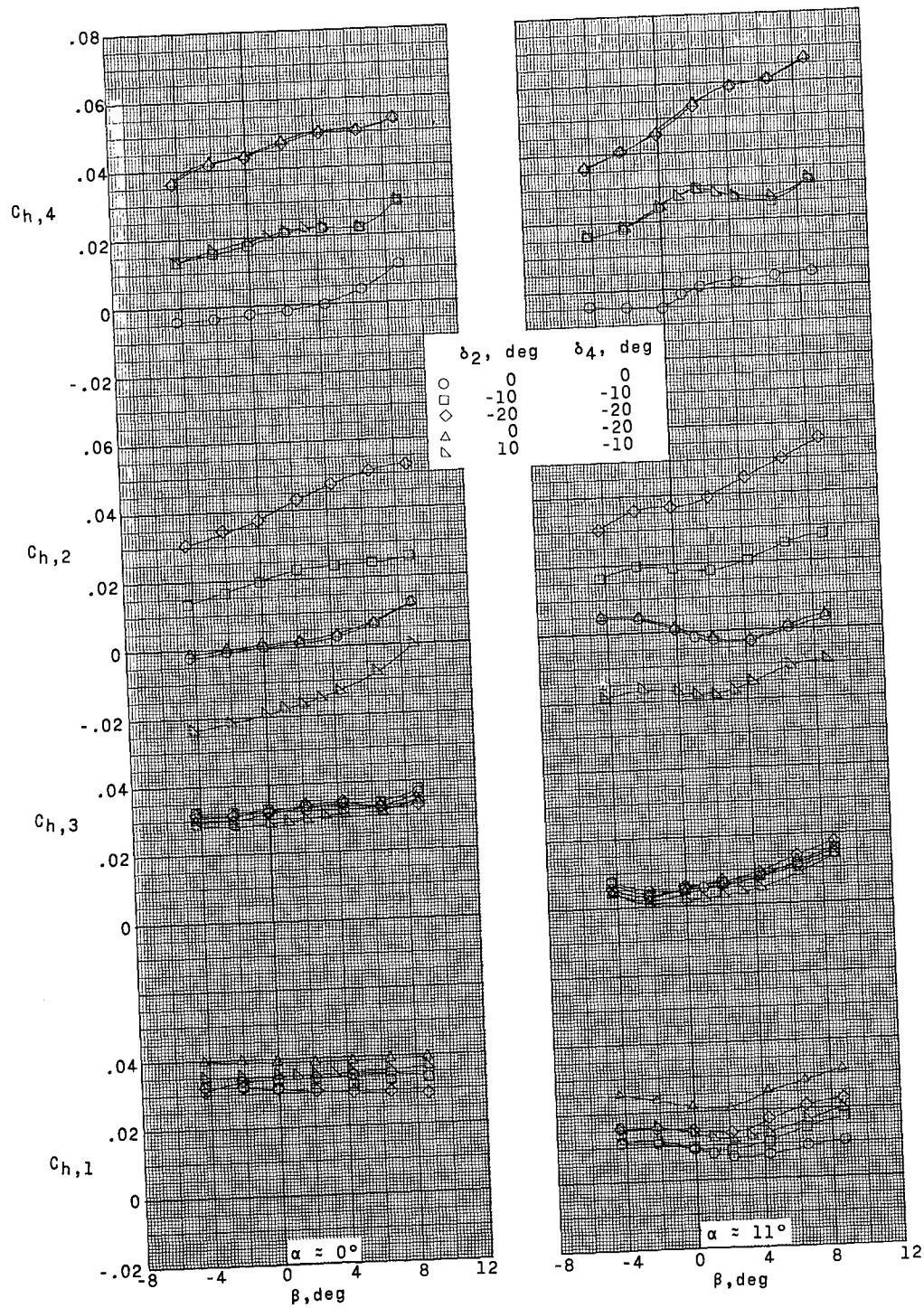
(b) M = 2.00.

Figure 6. - Continued.
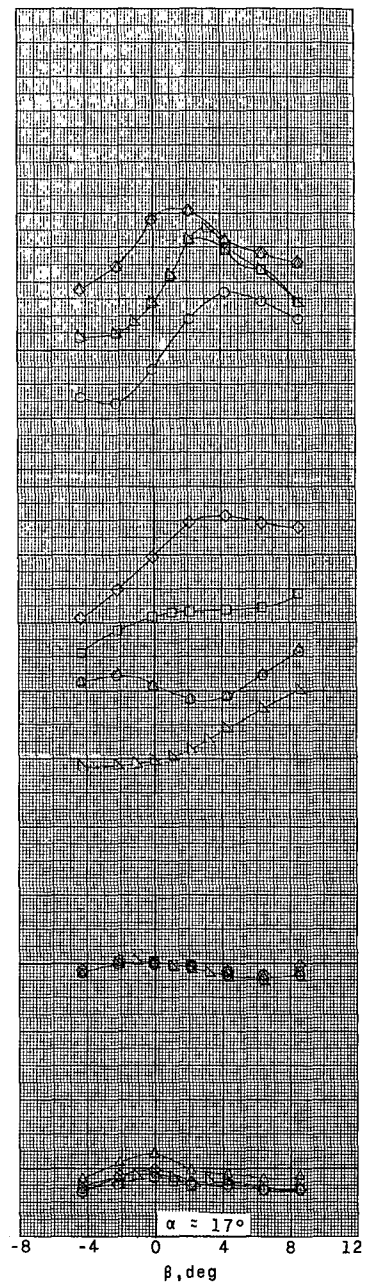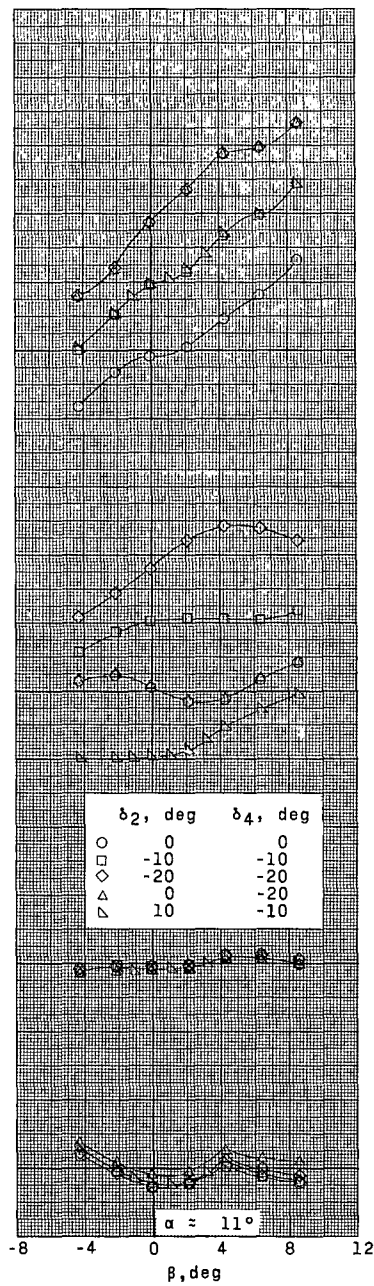
(c) M = 2.50.

Figure 6. - Concluded.

(a) M = 1.60.

Figure 7. – Effect of symmetrical and differential deflections of directional controls on lateral aerodynamic characteristics. $\delta_1 = \delta_3 = -20^\circ$; $\beta = 0^\circ$.

(b) M = 2.00.

Figure 7.- Continued.

δ_2, deg	δ_4, deg
○ 0	0
□ -10	-10
◇ -20	-20
△ 0	-20
◁ 10	-10

C_n

C_l

C_Y

α, deg

(c) M = 2.50.

Figure 7. – Concluded.

(a) M = 1.60.

Figure 8. – Hinge-moment characteristics for various control deflections. $\delta_1 = \delta_3 = 0^0$.
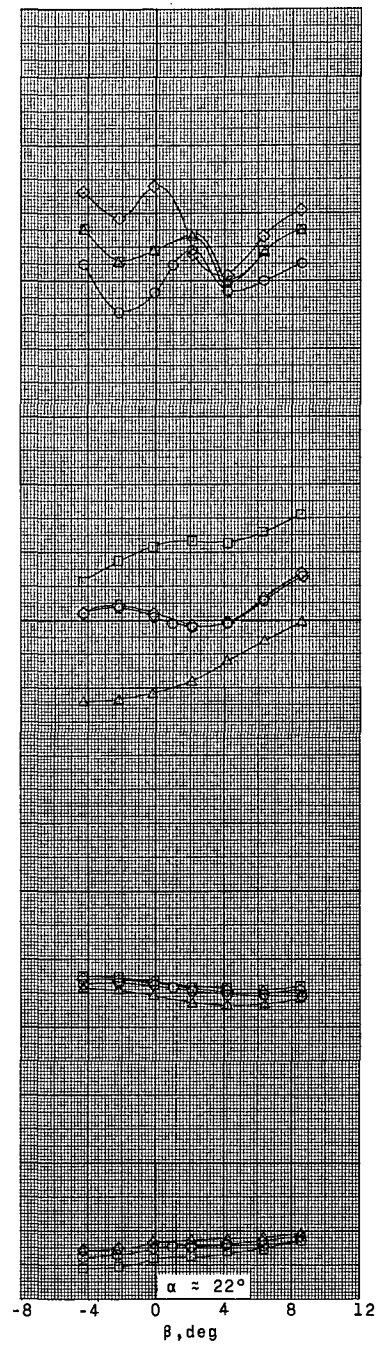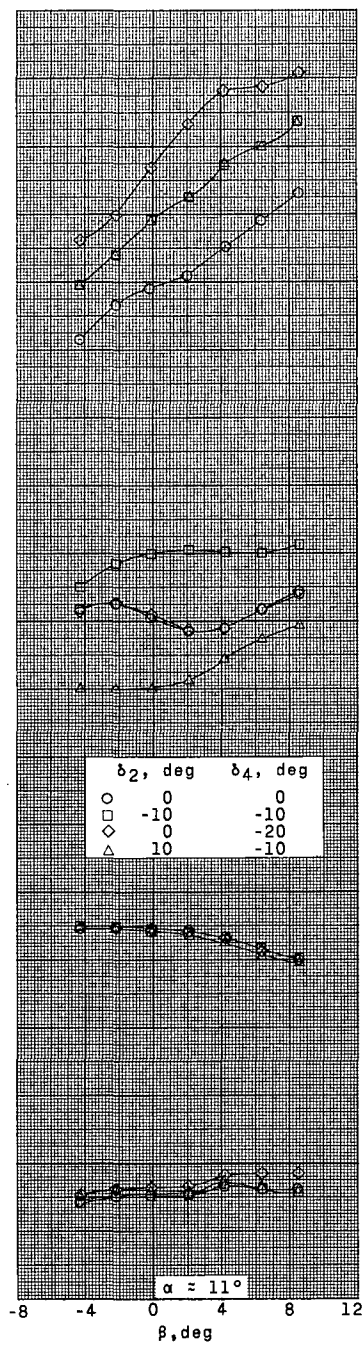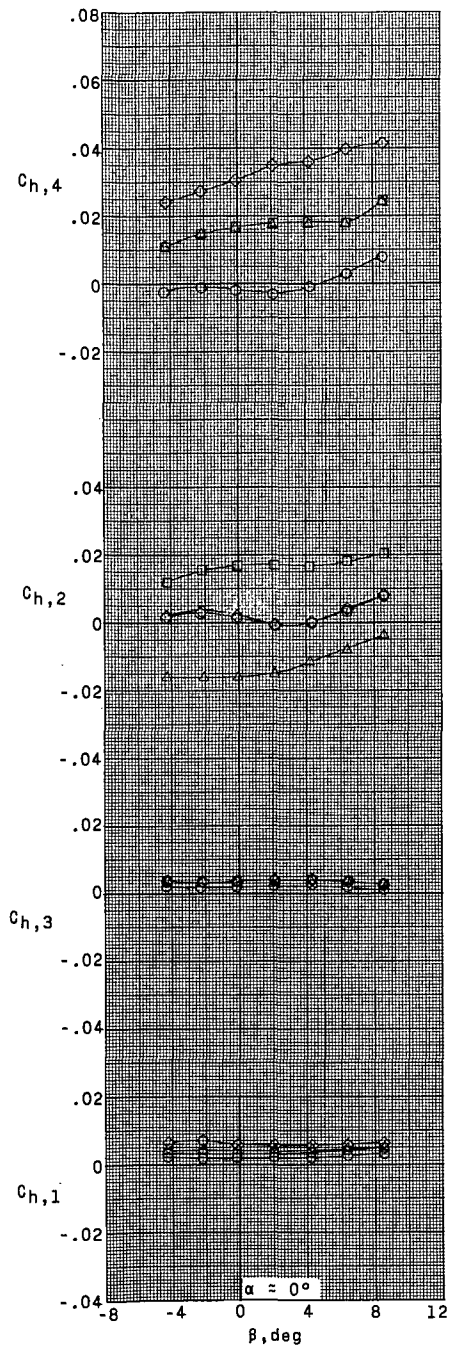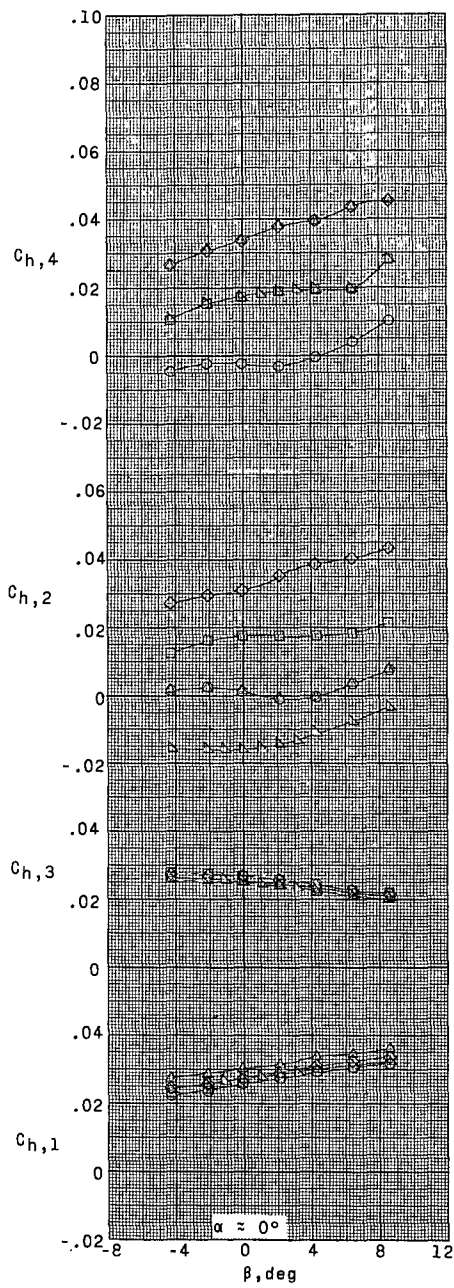
(b) M = 2.00.

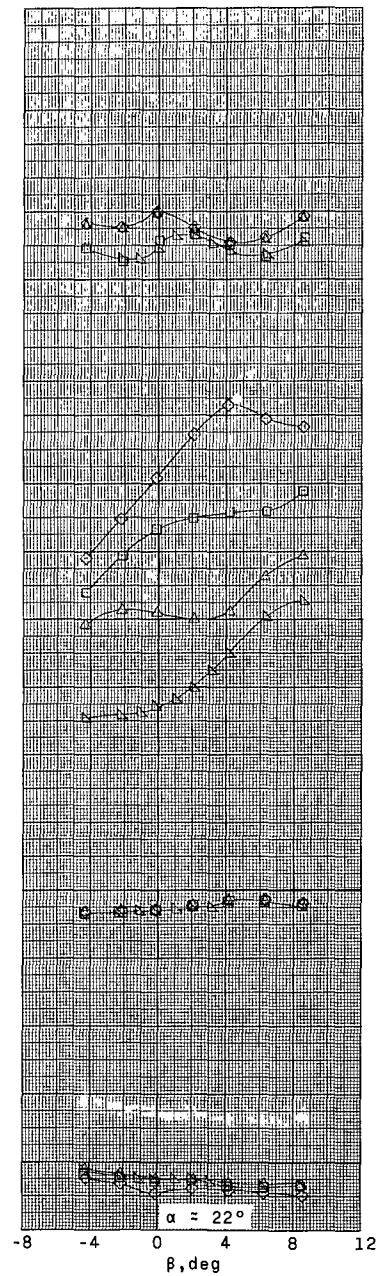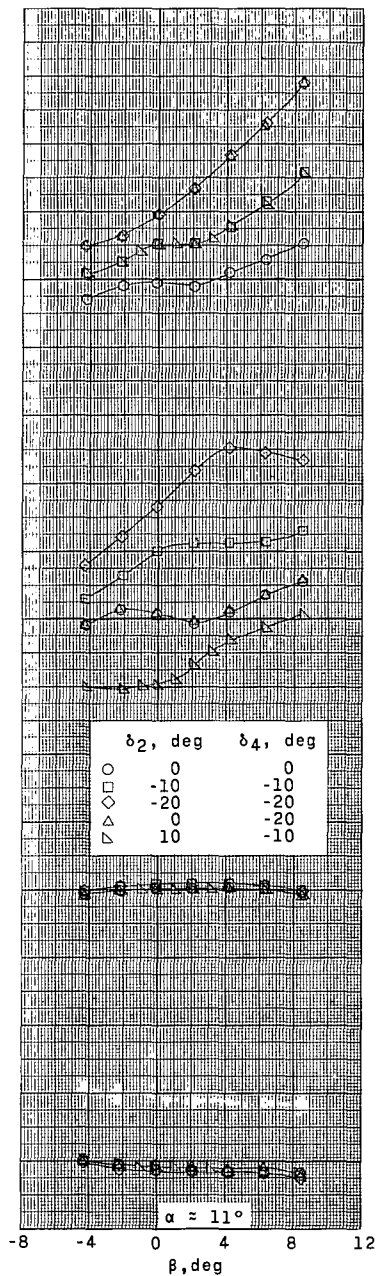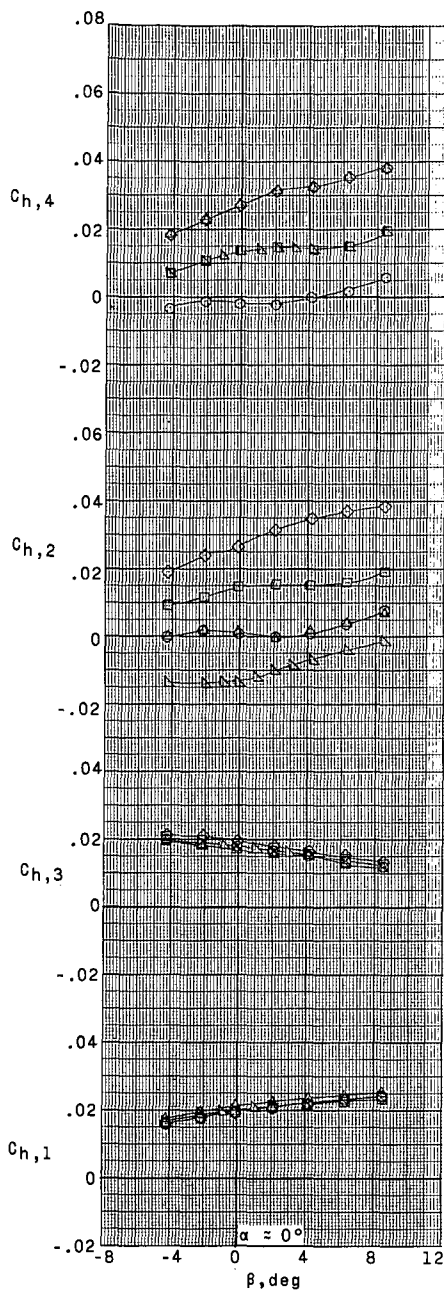Figure 8. - Continued.
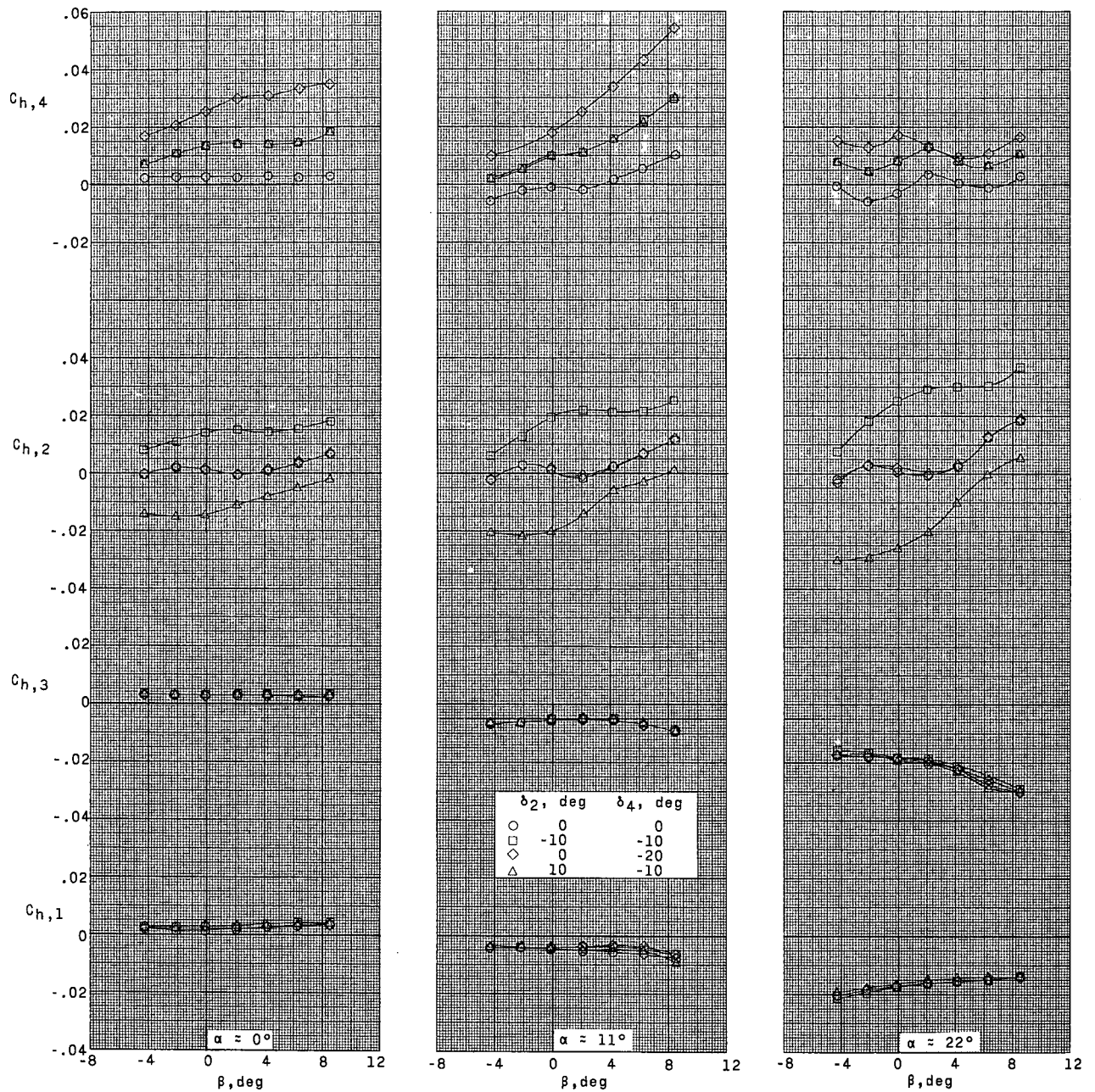
(c) M = 2.50.

Figure 8. - Concluded.

(a) M = 1.60.

Figure 9. - Hinge-moment characteristics for various control deflections. $\delta_1 = \delta_3 = -20^{\circ}$.

(b) M = 2.00.

Figure 9. - Continued.

(c) M = 2.50.

Figure 9. - Concluded.